Check for updates

Received: 15 December 2020 | Revised: 1 February 2021 | Accepted: 4 February 2021

DOI: 10.1002/ardp.202000473

FULL PAPER

ARCH PHARM DPhG
Archiv der Pharmazie

Design, synthesis, antibacterial evaluation, and computational studies of hybrid oxothiazolidin–1,2,4-triazole scaffolds

Prateek Pathak[1] | Jurica Novak[1] | Parjanya K. Shukla[2,3] | Maria Grishina[1] | Vladimir Potemkin[1] | Amita Verma[3]

[1]Laboratory of Computational Modeling of Drugs, Higher Medical and Biological School, South Ural State University, Chelyabinsk, Russia

[2]Krishnarpit Institute of Pharmacy, Dr. A. P. J. Abdul Kalam Technical University, Prayagraj, Uttar Pradesh, India

[3]Bioorganic and Medicinal Chemistry Research Laboratory, Department of Pharmaceutical Sciences, Sam Higginbottom University of Agriculture, Technology & Sciences, Prayagraj, Uttar Pradesh, India

Correspondence
Prateek Pathak, Laboratory of Computational Modeling of Drugs, Higher Medical and Biological School, South Ural State University, Chelyabinsk, Russia 454080.
Email: patkhakp@susu.ru and prateekpharm05@gmail.com

Amita Verma, Bioorganic and Medicinal Chemistry Research Laboratory, Department of Pharmaceutical Sciences, Sam Higginbottom University of Agriculture, Technology & Sciences, Prayagraj, Uttar Pradesh 211007, India.
Email: amitaverma.dr@gmail.com and amita.verma@shiats.edu.in

Funding information
Government of the Russian Federation, Grant/Award Numbers: Act 211, contract 02.A03.21.0011; Ministry of Science and Higher Education of Russia, Grant/Award Number: FENU-2020-0019

Abstract

Bacterial infections are a serious threat to human health due to the development of resistance against the presently used antibiotics. The problem of growing and widespread antibiotic resistance is only getting worse with the shortage of new classes of antibiotics, creating a substantial unmet medical need in the treatment of serious bacterial infections. Therefore, in the present work, we report 18 novel hybrid thiazolidine–1,2,4-triazole derivatives as DNA gyrase inhibitors. The derivatives were synthesized by multistep organic synthesis and characterized by spectroscopic methods (^{1}H and ^{13}C nuclear magnetic resonance and mass spectroscopy). The derivatives were tested for DNA gyrase inhibition, and the result emphasized that the synthesized derivatives have a tendency to inhibit the function of DNA gyrase. Furthermore, the compounds were also tested for antibacterial activity against three Gram-positive (*Bacillus subtilis* [NCIM 2063], *Bacillus cereus* [NCIM 2156], *Staphylococcus aureus* [NCIM 2079]) and two Gram-negative (*Escherichia coli* [NCIM 2065], *Proteus vulgaris* [NCIM 2027]) bacteria. The derivatives showed a significant-to-moderate antibacterial activity with noticeable antibiofilm efficacy. Quantitative structure–activity relationship (QSAR), ADME (absorption, distribution, metabolism, elimination) calculation, molecular docking, radial distribution function, and 2D fingerprinting were also performed to elucidate fundamental structural fragments essential for their bioactivity. These studies suggest that the derivatives **10b** and **10n** have lead antibacterial properties with significant DNA gyrase inhibitory efficacy, and they can serve as a starting scaffold for the further development of new broad-spectrum antibacterial agents.

KEYWORDS
antibacterial activity, DNA gyrase inhibitors, docking study, hybrid 1,2,4-triazole, QSAR study

Prateek Pathak and Parjanya K. Shukla contributed equally to this study.

 © 2021 Deutsche Pharmazeutische Gesellschaft

1 | INTRODUCTION

Bacterial infections are a persistent and increasing threat to human health due to the development of resistance against presently used antibiotics.[1–3] The problem of growing and widespread antibiotic resistance is only getting worse with the shortage of new classes of antibiotics, creating a substantial unmet medical need in the treatment of serious bacterial infections.[4,5] In a survey, worldwide, approximately half a million people have been infected by multidrug-resistant *Mycobacterium tuberculosis*, *Neisseria gonorrhoeae*, or *Pseudomonas aeruginosa* infections.[3,6,7] Therefore, the need for the development of effective antibacterials has become essential to control the spread of superbug microorganisms. The designing of novel antibacterial agents with a diverse mechanism of action could be a possible approach to overcome this resistance.[8] DNA topoisomerase enzymes participate in interconversion, relaxation, and supercoiling of DNA fragments.[9,10] They also act remarkably in various physiological functions such as replication, transcription recombination repair, and chromosome decondensation.[11,12] Structurally, DNA gyrase is a type IIA topoisomerase, belonging to the family of heat-shock protein 90 (Hsp 90), histidine kinase, MutL (GHKL), protein kinases, and the DNA mismatch repair protein MutL (mismatch from replication recognized by MutL).[12,13] It consists of two subunits, that is, GyrA and GyrB. DNA gyrase functions involve the coupling of GyrB subunit to supercoiling of DNA through ATP hydrolysis and maintain the DNA topology during the replication process.[14] Generally, DNA gyrase employs inhibition of bacterial growth via two main mechanisms: stabilization of the covalent enzyme–DNA complex (as ciprofloxacin) or blocking the ATP binding site of DNA gyrase B (as novobiocin).[15] It is considered as one of the crucial enzymes across the entire bacterial species and its inhibition results in disruption of DNA synthesis, followed by cell death. Thus, DNA gyrase inhibition is one of the most validating approaches in antibacterial chemotherapy.[16] Nowadays, the concept of hybrid molecules is very popular, in which two or more structural domains are conjugated and novel compounds possess different or dual pharmacological activity.[5,17] The drugs developed by this approach have the ability to reduce toxicity, overcome drug resistance, and improve optimal pharmacokinetic profiles.[18,19] Till date, several compounds synthesized by the hybrid approach are under clinical studies for their potential against various health-related issues such as abdominal infections, urinary tract infections, and pneumonia.[5,17,20] Heterocyclic skeletons are the main fragments of many marketed drugs, and they also play an important role in antibacterial activity, as found in contemporary drug discovery.[5] Compounds containing 1,2,4-triazole scaffold can impact lipophilicity, polarity, hydrogen bonding capacity, pharmacological, pharmacokinetic, toxicological, and physicochemical properties.[5,21] 1,2,4-Triazole-derived compounds customarily represent vital therapeutic classes that parade a broad spectrum of pharmacological actions such as anticancer,[22,23] antiviral,[24] antitubercular,[25] anti-inflammatory,[26] antifungal,[27,28] and antibacterial[29] activities. Studies show that substituents on the triazole nucleus at the different positions within the ring can be changed according to the desired derivatives designing, but the maximum antimicrobial properties are exerted by the groups attached to the nitrogen atom at the first position.[30] Therefore, during the designing of novel 1,2,4-triazole-based compounds, the position of the nitrogen atom should be fixed according to its suggested structure–activity relationship (SAR). 4-Oxo-thiazolidines are the derivatives of thiazolidinone with a carbonyl group at position 4 formed by the attack of sulfur nucleophile on imine carbon, followed by intramolecular cyclization with the elimination of water.[31] The nucleus of 4-oxo-thiazolidine derivatives has a distinctive place in medicinal chemistry due to its wide range of diverse pharmacological activities such as antimicrobial,[32,33] antidiabetic,[34] anti-HIV,[35] enzyme murB inhibition,[36] antitubercular,[37] and anticancer.[32]

In this study, we considered the abovementioned phenomena of both heterocyclic skeletons and decided to synthesize 1,2,4-triazole derivatives via the hybridization with thiazolidin skeleton as potential antibacterial compounds. Moreover, the hybrid 1,2,4-triazole-conjugated 4-oxo-thiazolidins were evaluated for their antibacterial efficacy against five bacterial strains, followed by ADMET (absorption, distribution, metabolism, elimination) properties calculations, molecular docking, and quantitative structure–activity relationship (QSAR) studies.

2 | RESULTS AND DISCUSSION

2.1 | Chemistry

We have synthesized a series of derivatives by conjugating 1,2,4-triazole and the thiazolidine scaffolds to probe the SAR of hybrid 1,2,4-triazole–thiazolidins. The complete synthetic procedure is composed of the traditional seven steps of organic synthesis (Schemes 1 and 2). The first step (reaction i) includes Fischer esterification, where substituted aromatic carboxylic acids **1a–c** were refluxed with methanol in the presence of sulfuric acid to afford the intermediate aromatic acid esters (**2a–c**). Furthermore, in the next step (reaction ii), the intermediates (**2a–c**) participated in the formation of acid hydrazides (**3a–c**) through the attachment of the hydrazide group via a classical addition reaction. The third synthetic protocol (reaction iii) corresponds to the formation of substituted dithiocarbazinic acid salts (**4a–c**) through the addition of carbon disulfide (CS_2)/KOH with **3a–c** and dithiocarbazinic acid salts. In the next reaction step (reaction iv), 1,2,4-triazole scaffolds (**5a–c**) were synthesized under reflux using hydrazine hydrate.[26] Furthermore, in the reaction v, 2-chloro-*N*-(5-mercapto-3-substituted phenyl-1,5-dihydro-4*H*-1,2,4-triazol-4-yl) (**6a–c**) were synthesized by the electrophilic substitution of chlorine atom from the chloroacetyl chloride in the presence of sodium acetate and glacial acetic acid. In reaction vi, the addition of hydrazine hydrate with *N*-(5-aryl-1,2,4-triazole-2-yl)-2-chloroacetamide (**6a–c**) in the presence of methanol offered the synthesis of 2-hydrazinyl-*N*-(5-mercapto-3-substituted phenyl-1,5-dihydro-4*H*-1,2,4-triazol-4-yl)acetamides (**7a–c**). In the final step

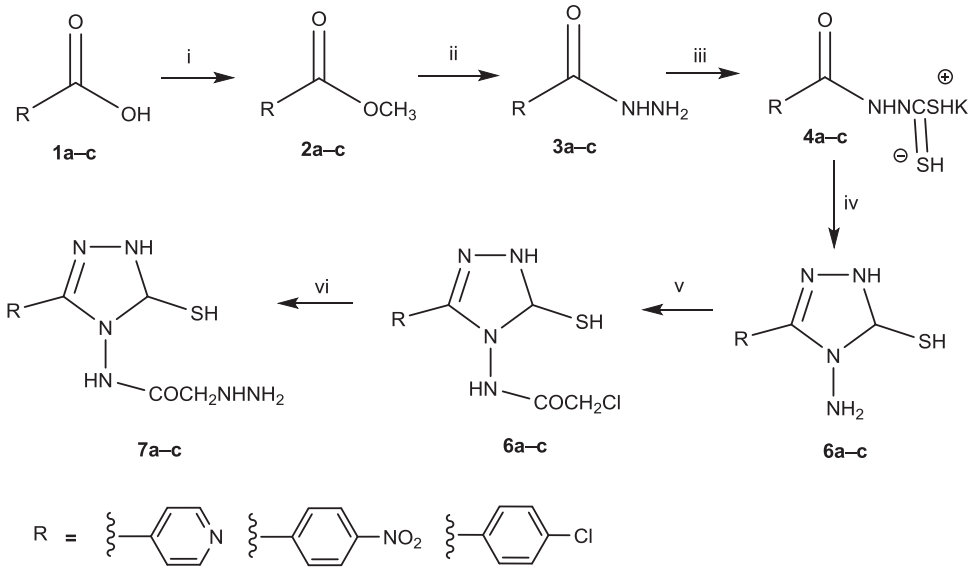

SCHEME 1 The reaction scheme for the synthesis of the 1,2,4-triazol precursors. Reagents and conditions: (i) carboxylic acid, methanol, conc. H_2SO_4, reflux for 8–10 h, (ii) hydrazine hydrate, methanol, reflux for 3 h, (iii) KOH, carbon disulfide, stirring for 16 h at room temperature, (iv) hydrazine hydrate, H_2O, stirring, and reflux for 3 h, (v) glacial acetic acid, saturated solution of sodium acetate, chloroacetyl chloride, stirring for 3 h, (vi) hydrazine hydrate, ethanol, stirring for 20–30 min

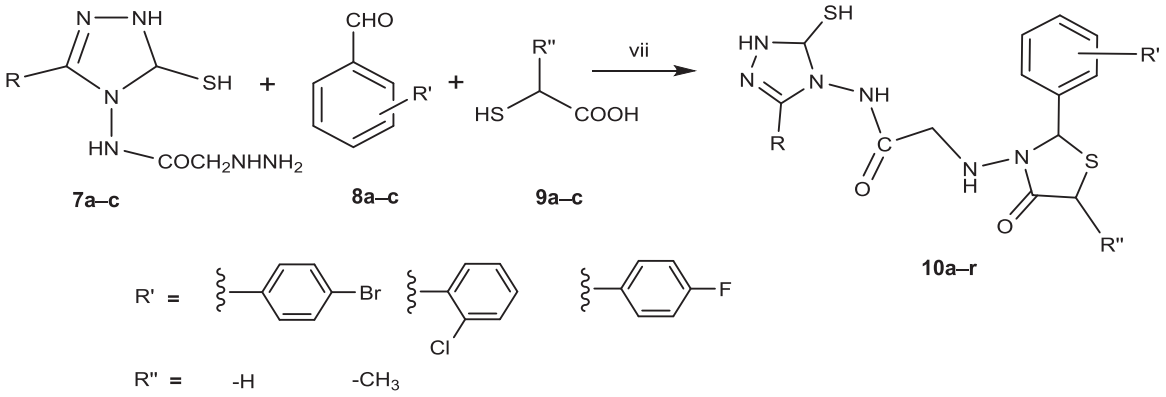

SCHEME 2 Scheme for the synthesis of the final hybrid oxo-thiazolidin–1,2,4-triazole compounds. Reagents and conditions: (vii) substituted benzaldehydes, substituted thioglycolic acid, $ZnCl_2$, ethanol, reflux for 6–7 h

(reaction vii), the heterocyclic skeletons 2-hydrazinyl-*N*-(5-mercapto-3-substituted phenyl-1,5-dihydro-4*H*-1,2,4-triazol-4-yl)acetamides (**7a–c**) were condensed with benzaldehydes (**8a–c**) and thioglycolic acid derivatives (**9a–c**) under reflux in the presence of $ZnCl_2$. Finally, the aimed derivatives 2-[2-(substituted-phenyl)-5-substituted-4-oxo-thiazolidin-3-ylamino]-*N*-[5-mercapto-3-(substituted-phenyl)-1,5-dihydro-1,2,4-triazol-4-yl]acetamides (**10a–r**) were obtained and the structural conformations were performed by ^{1}H nuclear magnetic resonance (NMR), ^{13}C NMR, and elemental analysis. ^{1}H NMR showed a singlet at δ 1.52 and δ 3.943 ppm, which are attributed to the presence of SH and CH_2 protons. CH peaks of the thiazolidine and triazole appeared at 6.296 and 6.426 ppm. CH groups of aromatic rings appeared as doublets between δ 7.16–7.12 and δ 8.12–8.09 ppm. Two different characteristic singlets in the range of δ 8.87–9.13 ppm confirmed the presence of various NH groups. The ^{13}C NMR spectrum of all the derivatives showed the presence of six carbon atoms of the aromatic ring in the region of 115.1–167.2 ppm, five pyridine carbon peaks in the range of 121.3–149.6 ppm, and one carbon of CH_2 at 66.6 ppm. Elemental analysis confirmed that the presence of carbon, hydrogen, and nitrogen in all derivatives is in accordance with expected values.

2.2 | Antibacterial activity

The entire series of derivatives were screened for their minimum inhibitory concentration (MIC, μg/ml) against a panel of three Gram-positive and two Gram-negative bacterial strains (details are provided in Section 4) for determination of antibacterial efficacy, and results are depicted in Table 1. The present study included

TABLE 1 Antibacterial and antibiofilm activity of the derivatives

Compound	Minimum inhibitory concentration (μg/ml)					Antibiofilm activity (μg/ml)
	Bacillus subtilis	*Bacillus cereus*	*Staphylococcus aureus*	*Escherichia coli*	*Proteus vulgaris*	*Staphylococcus aureus*
10a	25	>50	25	12.5	25	50
10b	6.25	12.5	3.125	25	6.25	25
10c	12.5	25	12.5	ND	25	75
10d	12.5	50	12.5	25	25	75
10e	6.25	6.25	6.25	6.25	25	100
10f	6.25	12.5	6.25	12.5	12.5	50
10g	12.5	6.25	6.25	25	25	100
10h	6.25	25	6.25	50	12.5	75
10i	12.5	25	12.5	25	50	100
10j	25	>50	25	6.25	50	100
10k	12.5	12.5	12.50	25	>50	50
10l	>50	ND	>50	12.5	12.5	100
10m	12.5	6.25	12.5	12.5	25	75
10n	6.25	3.125	3.125	25	12.5	12.5
10o	6.25	6.25	6.25	12.5	25	25
10p	25	25	12.5	12.5	50	25
10q	25	12.5	25	ND	>50	100
10r	12.5	6.25	12.50	25	25	50
Ciprofloxacin	6.25	3.125	3.125	6.25	3.125	25

Abbreviation: ND, not determined.

ciprofloxacin as a reference antibacterial agent for comparing the effectiveness of synthesized derivatives. On the basis of SAR (Figure 1), it is important to indicate that the presence of nitrobenzene substituent (at the position R) has a noticeable effect on the activity profile, as seen in the case of compound **10b**. Its activity has been increased as compared with its pyridine counterpart, compound **10a**. However, the replacement of nitro group with chloro (in compound **10c**) slightly lowers the antibacterial potency against all tested bacterial species. Compound **10d** was derived through the slight alteration (addition of methyl group at R″) in the thiazolidine skeleton of **10a**, and it shows a slight improvement in the activity against *Bacillus subtilis* (MIC = 12.5 μg/ml) and *Staphylococcus aureus*

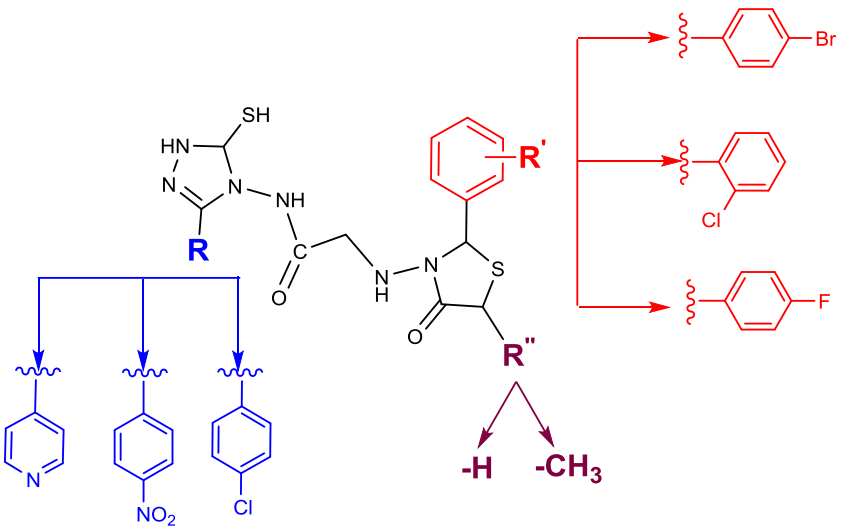

FIGURE 1 General structure of the hybrid derivatives

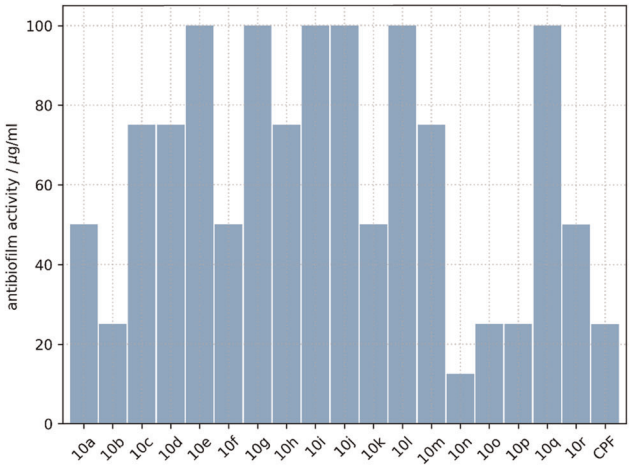

FIGURE 2 Antibiofilm activity of the hybrid derivatives. CPF, ciprofloxacin

(MIC = 12.5 μg/ml), but lowers the activity against *Escherichia coli* (MIC = 25 μg/ml). Hydrogen to methyl group mutation at the position R″ does not influence the activity against *Bacillus cereus* (MIC = 50 μg/ml) and *Proteus vulgaris* (MIC = 25 μg/ml) as compared with **10a**, and it is found as slightly more active compared with the standard and **10c**. Compound **10e** was constructed through the substitution of hydrogen by a methyl group (at R″) on the thiazolidine ring of **10b**, and it illustrates a higher potency against *B. cereus* (MIC = 6.25 μg/ml) and *E. coli* (MIC = 6.25 μg/ml). A significant upsurge in antibacterial activity against tested microorganisms was reported by **10f** having electron-withdrawing groups at both the positions (at R and R′). The addition of chlorobenzene to the 1,2,4-triazole skeleton (at R′) and substitutions by different fragments introduced to the thiazolidine ring at position R resulted in the derivatives **10g–i**.

The assay showed that the derivatives **10g–i** have moderate antibacterial potency (ranging from 6.25 to 25 μg/ml) against the tested microorganism. The introduction of CH_3 group on the thiazolidine ring of compounds **10g–i** resulted in derivatives **10j–l** and is accompanied by a slight reduction in the antibacterial potency. The derivatives **10m–o** contain common fluorobenzene ring on thiazolidine fragment (at position R′). The different substitution occurs on 1,2,4-traizole scaffolds (pyridine, nitrobenzene, chlorobenzene at position R, respectively). The antibacterial evaluation showed that compound **10m** has moderate inhibition potency. Compound **10n** was found equipotent as standard, ciprofloxacin, against *B. subtilis*, *B. subtilis*, and *S. aureus*, and less active against *P. vulgaris* and *E. coli*. Hybrid compound **10o** displayed equipotent efficacy as a standard against *B. subtilis* and moderate activity against the rest of the tested bacterial strains. Addition of methyl group on the thiazolidine fragment of the derivative **10m** constructed **10p**, a molecule that displayed a notable drop in antibacterial potency. Repeatedly, it was found that the addition of methyl side chain on thiazolidine ring leads to lowering the antibacterial efficacy. Compound **7q** was synthesized through the introduction of nonhalogenated electron-withdrawing group on 1,2,4-triazole (addition of nitrobenzene), and it showed a radical drop in activity against an entire set of tested microorganisms. The overall results depicted that the entire set of synthesized hybrid derivatives exhibited mild-to-moderate activity, whereas derivatives **10b** and **10n** showed potent inhibition against tested bacterial strains. On the basis of the antibacterial evaluation outcomes, SAR studies suggested that the nature of substituents has a strong impact on the antibacterial activity. It has been demonstrated that the introduction of strong electron-withdrawing groups makes derivatives more active against tested bacterial strains. Thus, it could be understood that these perturbations caused by electron-withdrawing groups (such as halogen) are very useful to modulate the steric effect on the phenyl ring of the drug and facilitate the molecules to enter the bacterial cell wall.[38]

2.3 | Antibiofilm activity

The hybrid derivatives exhibiting antibacterial properties were also screened for bacterial biofilm inhibition against *S. aureus*. The result is displayed in Table 1 and Figure 2.

The main result is that the derivatives inhibit the biofilm formation with IC_{50} values ranging between 25 and 100 μg/ml with mild-to-moderate potential. Compounds **10n** and **10b** were found to be the most effective (12.5 and 25 μg/ml, respectively) among the entire set of tested derivatives, whereas derivative **10n** has higher potential as equated with ciprofloxacin.

2.4 | Inhibition of DNA gyrase supercoiling activity

In this section, we present the determination of the inhibitory potential of the newly synthesized hybrid derivatives against DNA gyrase enzyme. The results are given in terms of IC_{50}, compared with the ciprofloxacin as standard (Figure 3). The hybrid

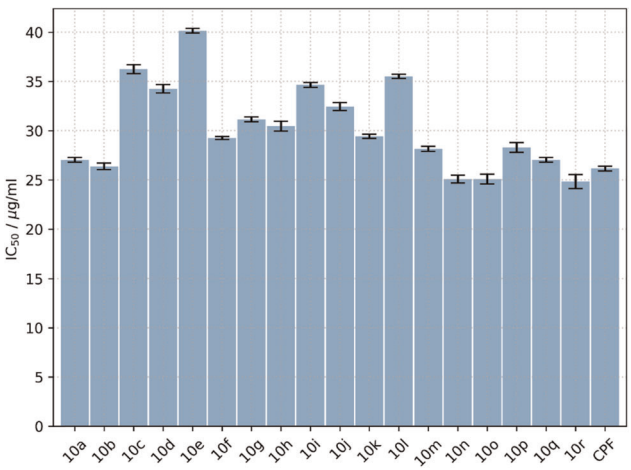

FIGURE 3 *Staphylococcus aureus* DNA gyrase inhibitory activity of the hybrid derivatives. CPF, ciprofloxacin

thiazolidine–triazole derivatives have moderate-to-significant inhibitory potential, with derivatives **10b**, **10n**, **10o**, and **10r** being the maximum effective (with IC_{50} values of 26.36 ± 0.33, 25.06 ± 0.4, 25.09 ± 0.5, and 24.84 ± 0.71 μg/ml, respectively).

Furthermore, a slight decline in inhibition was reported for derivatives **10a** (IC_{50} = 27.03 ± 0.24 μg/ml), **10f** (IC_{50} = 29.25 ± 0.15 μg/ml), **10k** (IC_{50} = 29.42 ± 0.22 μg/ml), **10m** (IC_{50} = 28.15 ± 0.25 μg/ml), **10p** (IC_{50} = 28.28 ± 0.5 μg/ml), and **10q** (IC_{50} = 27.03 ± 0.24 μg/ml). For derivatives **10c**, **10d**, **10e**, **10g**, **10h**, **10i**, **10j** and 10l, IC_{50} decreases and displayed above 30 μg/ml. The standard drug ciprofloxacin that was used for the comparison of efficacy exhibited IC_{50} at 26.15 ± 0.25 30 μg/ml. Other researchers also illustrated the DNA gyrase inhibition potency of ciproflaxacin at similar concentration.[39] This study suggests that the introduction of electron-withdrawing group increases the DNA gyrase inhibitory potential, which is found to be in accordance with the in vitro antibacterial activity assay. On the basis of the similarity of antibacterial activity and DNA gyrase inhibition results, it can be concluded that the synthesized derivatives may act as DNA gyrase inhibitors and produce their antibacterial activity typically through its DNA gyrase inhibition mechanism.

2.5 | Three-dimensional (3D) QSAR studies

3D QSAR studies are important methods in modern novel drug design and their results can guide the synthesis of future compounds with desired properties. In the current study, one such method was used to elucidate key derivatives features, important for their antibacterial activity. The distribution of pharmacophore (red), antipharmacophore (blue), and inactive parts (gray) of the most promising compounds, **10b** and **10n**, are displayed in Figure 4. The gray part of the ring does not participate in pharmacological activity, but is important for configuring the chemical structure. The assay illustrates that hydrogen atoms within the entire section of compounds act as pharmacophoric parts. The sulfur and oxygen atoms in the thiazolidine ring and oxygen atom of the acetamide bridge act as antipharmacophoric parts. As suggested by directional structural changes aimed at increasing biological activities, these antipharmacophoric atoms can be replaced by any suitable pharmacophoric group.

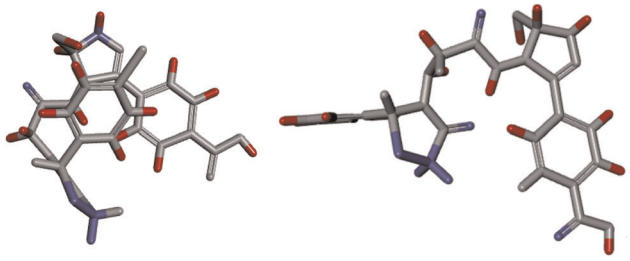

FIGURE 4 Pharmacophore (red), antipharmacophore (blue), and ballast (gray) parts of the derivatives **10b** (left) and **10n** (right)

Radial distribution function (RDF) weighted by the number of valence shell electrons for all synthesized molecules have two well-resolved maxima at 1.4 and 2.5 Å (Figure 5, left). This corresponds to the approximate carbon–carbon bond length (1.4 Å) and the distance between two carbon atoms sharing the same neighbor (2.5 Å). The highest standard deviation of the RDF is at the distance of 8.6 Å, reaching 63% of the mean RDF value at that distance (Figure 5, right).

This fact reflects a different orientation of the same (or similar) groups in space. For example, compounds **10b** and **10n** differ only by the type of halogen atom on *para* position of benzene ring on thiazolidine skeleton. By overlaying the nitrobenzene moieties of the two molecules (Figure S1), one can see that plains defined by nitrobenzene and fluorobenzene rings in **10n** are almost parallel, but are directed in opposite sides as compared with thiazolidin–1,2,4-triazole backbone. In the case of **10b**, both phenyl groups are from the same side of thiazolidin–1,2,4-triazole backbone. The changes in the geometry are captured by the RDF, as can be seen from Figure 5, where RDF for **10b** and **10n** is highlighted. The intrinsic property of the RDF is that it unambiguously describes the arrangement of the atoms in 3D space, plus it is invariant against the translation and rotation of a molecule. Therefore, it is a perfect candidate as a structure-related descriptor in the investigation of the relationship between structure and relevant properties in drug design. A three-parameter (plus intercept) regression model correlating the RDF descriptors and IC_{50} values is developed:

$$IC_{50} = 42.29226372 - 0.01683116g_{5.5} + 0.05702761g_{6.0} - 0.06652460g_{6.2}. \quad (1)$$

The model has the coefficient of determination (R^2) of .661 and standard error of the estimate of 2.8. g_r represents the value of the RDF descriptor at distance r. The plot of the experimentally determined versus IC_{50} values predicted by Equation (1) is graphically presented in Figure 6.

2.6 | Absorption, distribution, metabolic liability prediction, and excretion studies

From the last few decades, in silico ADME studies are found to be more beneficial than wet experiments, due to reduction of cost and time. In the current section, the derivatives were evaluated for their ADME properties to elucidate key features, which have importance in antibacterial activity (Table 2).

Briefly, the results showed that all synthesized derivatives have log *P* values <5, low tendency to be absorbed through the gastrointestinal tract, optimal TPSA values (in the range of 180–212 $Å^2$), low number of violations of Lipinki's rule of five,[40] and they do not cross the blood–brain barrier. It is important to note that Lipinski's rules represent statistical guidelines for orally administered drugs, and there are numerous cases of orally available drugs that do not comply with all the rules, for example, cefozopran (Firstcin®) as a representative of cephalosporin[41] and azithromycin[42] and roxithromycin[43] as representatives of other well-known antibacterial

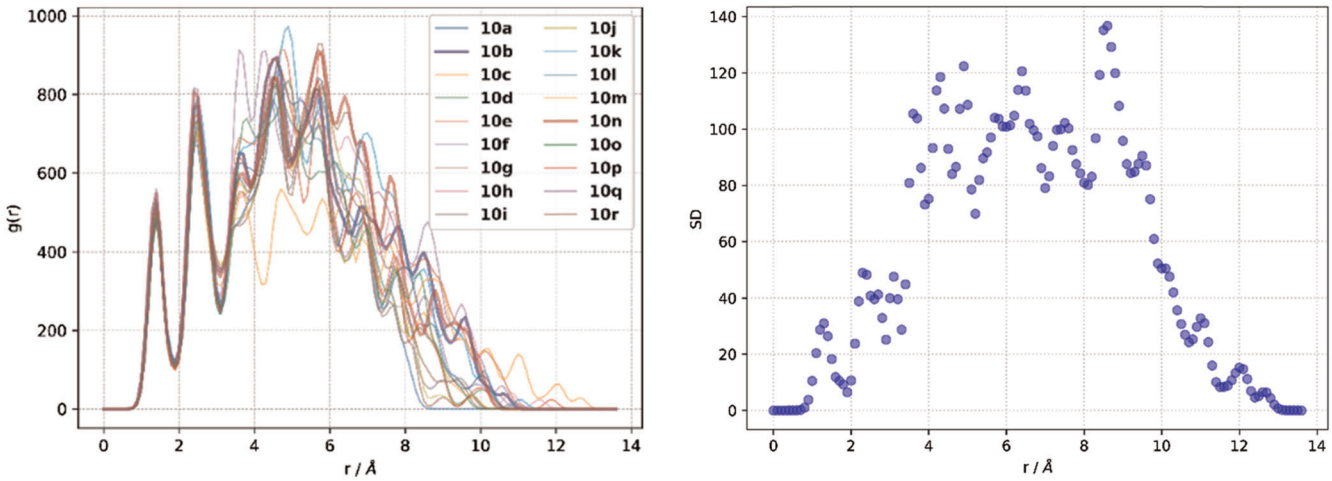

FIGURE 5 Radial distribution functiong (*r*) (left) and its *SD* (right) for a series of hybrid oxothiazolidin–1,2,4-triazole compounds

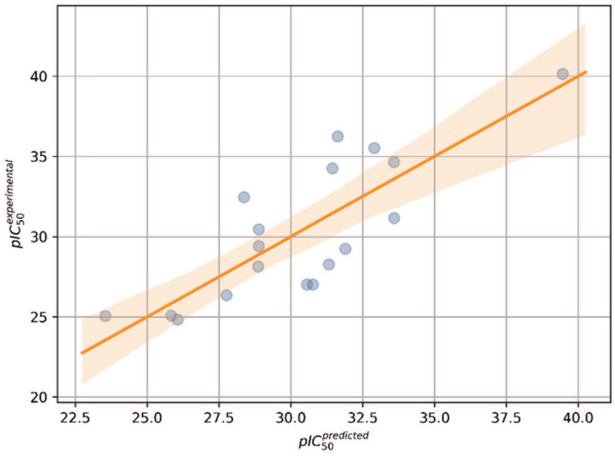

FIGURE 6 Experimentally observed versus predicted IC_{50} values using Equation (1), with 95% confidence interval

drugs. Moreover, clinically used drugs are subjected to metabolism in vivo, which increases the degradation of the molecule into the various fragments and increases polarity for excretion. The metabolic processes are also related to the production of toxic byproducts. In the early stage of drug discovery, the site of metabolism (SOM) of drug candidate is very vital, and its prediction could prevent recapitulation in the subsequent stages and reduce the possible liabilities and risks coupled with biotransformation.[38] As we found that the synthesized scaffolds have a promising antibacterial activity, it was worthy to define its metabolic liability. Although the metabolites of our synthesized compounds and their reactivity are still unknown (a step performed in later stages in the drug development), it is important to assess the metabolism of the parent compounds by CYP enzymes, to avoid pharmacokinetic interactions. In the present study, we have utilized two diverse programs, pkCSM[44] and RS-Predictor,[45] for the prediction of metabolism. The pkCSM was used to recognize the possibility of metabolism of synthesized compounds at different sites of cytochrome P450 isozyme (3A4, 1A2, 2C19, 2C9, and 2D6), and the results are displayed in Table 2. Metabolism prognosis for different CYP enzymes showed that the entire set of compounds is not metabolized at the site of CYP2D6 and CYP1A2. For other CYP enzymes (namely 3A4, 2C19, and 2C9), the results are mixed, but what is important is that the least active compounds (**10a**, **10g**, **10j**, and **10m**) are not predicted to be metabolized by CYP3A4, which was found in accordance with other standard chemotherapeutic agents clarithromycin, erythromycin, itraconazole, ketoconazole, ritonavir, and verapamil.[46] Therefore, there is a large possibility that these active molecules can serve as a good starting point for the further development of active antibacterial agents. The RS-Predictor[45] was utilized to identify the SOM and its probabilities to metabolize at each CYP isozyme (1A2, 2A6, 2B6, 2C8, 2C9, 2C19, 2D6, 2E1, and 3A4). The most probable SOM of the most active compound **10b** and the rest of the compounds are displayed in Figures 7 and S2, respectively. In the entire series, the sulfur atom of thiazolidine is highly labile as the SOM, except in the case of CYP2AB6 isozyme. Other fragments of the molecule were identified as moderately and fairly labile. Organic cation transporter 2 is a renal uptake transporter that plays an important role in the disposition and renal clearance of drugs and endogenous compounds. Thus, the assessment of OCT2 of any drug candidate provides useful information about clearance.[44] The prognosis showed that most effect derivatives **10b** and **10n** have a lower tendency to transport from OCT2 pathway, which need to be investigated further from in vivo studies. Due to lipophilic character and minimal tendency to transport from OCT2 pathway, it can be predicted that derivatives **10a**, **10b**, **10d**, **10g**, **10h**, **10j**, **10m**, **10n**, **10p**, and **10q** can effectively bind with serum/plasma and could participate in long-lasting therapeutic effect.

2.7 | Molecular docking experiments

Being aware of the advantages and issues of molecular docking experiments,[47] we performed docking of synthesized hybrid

TABLE 2 Physiochemical properties (ADME) calculation of synthesized derivatives

Compound	log *P*	GI abs	Lip vio	H acc	H don	TPSA	BBB per	Metabolism at CYP450					Renal OCT2 substrate
								3A4	1A2	2C19	2C9	2D6	
10a	1.4	L	1	9	4	190	−1.6	N	N	N	N	N	N
10b	1.9	L	2	10	4	206	−1.6	Y	N	N	Y	N	N
10c	2.7	L	1	8	4	201	−1.5	Y	N	Y	Y	N	Y
10d	1.8	L	1	9	4	197	−1.6	Y	N	N	N	N	N
10e	2.3	L	2	10	4	212	−1.6	Y	N	N	N	N	Y
10f	3.1	L	1	8	4	208	−1.5	Y	N	Y	Y	N	Y
10g	1.3	L	0	9	4	187	−1.5	N	N	N	N	N	N
10h	1.8	L	2	10	4	202	−1.5	Y	N	N	Y	N	N
10i	2.6	L	0	8	4	198	−1.5	Y	N	N	N	N	Y
10j	1.7	L	0	9	4	193	−1.6	N	N	N	N	N	N
10k	2.2	L	2	10	4	208	−1.5	Y	N	N	N	N	Y
10l	2.9	L	1	8	4	204	−1.4	Y	N	N	Y	N	Y
10m	0.81	L	0	9	4	180	−1.5	N	N	N	N	N	N
10n	1.3	L	1	10	4	196	−1.5	Y	N	N	Y	N	N
10o	2.1	L	0	8	4	192	−1.5	Y	N	N	N	N	Y
10p	1.1	L	0	9	4	187	−1.6	Y	N	N	N	N	N
10q	1.7	L	2	10	4	202	−1.5	Y	N	N	N	N	N
10r	2.4	L	0	8	4	198	−1.5	Y	N	N	Y	N	Y

Note: Log *P* is the logarithm of the octanol–water partition coefficient; GI abs, gastrointestinal absorption; Lip vio, total number of violation of Lipinski's rule of five; H acc, H acceptor; H don, H donor; TPSA, total polar surface area; columns 1A2, 2C19 2C9, 2D6, and 3A4 showed the metabolism on different isoforms of cytochrome-P450; renal OCT2 substrate, organic cation transporter 2; L, low; Y, likely to be metabolized; N, not likely to be metabolized.

molecules to the DNA gyrase's active site, with the intention to identify binding poses and to compare the binding energy with the known inhibitor ciprofloxacin. All docking results are compiled in Table 3. The top three compounds according to experimentally determined IC_{50} values against *S. aureus* DNA gyrase are **10r**, **10n**, and **10o**, respectively, and together with **10b**, they display a higher activity as compared with standard (ciprofloxacin). These results are in good agreement with our docking studies, where **10b**, **10n**, **10o**, and **10r** have the lowest predicted binding energy.

As compounds **10b** and **10n** are identified as hit molecules (they also have the highest anti-biofilm activity), their interaction pattern inside the DNA gyrase active pocket was analyzed in more detail (Figures 8 and S3). Derivative **10b** is positioned in the active site in a way that nitrobenzyl moiety is placed above nucleobases thymine (chain E) and adenine (chain H), and it establishes favorable aromatic stacking
interactions with thymine and hydrogen bridge with adenine.

On top of nitrobenzyl is guanine (chain G), so substituted 1,2,4-triazole substructure is actually intercalated between two subsequent base pairs. For crystal structure of DNA gyrase with ciprofloxacin in the active pocket (PDB ID: 2XCT), a similar pattern can be observed. An additional hydrogen bond between guanine (chain G) and carbonyl oxygen (**10b**) is formed. In compound **10n**, the bromine atom on the benzene ring of **10b** is replaced by fluorine. Due to this minor modification, in the most stable pose of **10n** inside the catalytic pocket, thiazolidine moiety with fluorobenzene is intercalated between nucleobases thymine (chain E) and guanine (chain G). 1,2,4-Triazole with nitrobenzene is anchored to protein pocket at the interface of two subunits. There are several FDA-approved drugs that exhibit a bactericidal action through the inhibition of topoisomerase II (DNA gyrase) and/or topoisomerase IV.[9] Therefore, to validate our results additionally, we selected and docked five known drugs and their precursor (nalidixic acid) to DNA gyrase (PDB ID: 2XCT), following the same protocol as for novel hybrid compounds (Table 3). All drugs demonstrate a similar affinity toward the enzyme and the predicted binding constants are comparable to binding constants of newly synthesized compounds. The binding score for nalidixic acid is −7.9 kcal/mol, showing how the optimization of the lead compound could lead toward inhibitors that are more efficient.

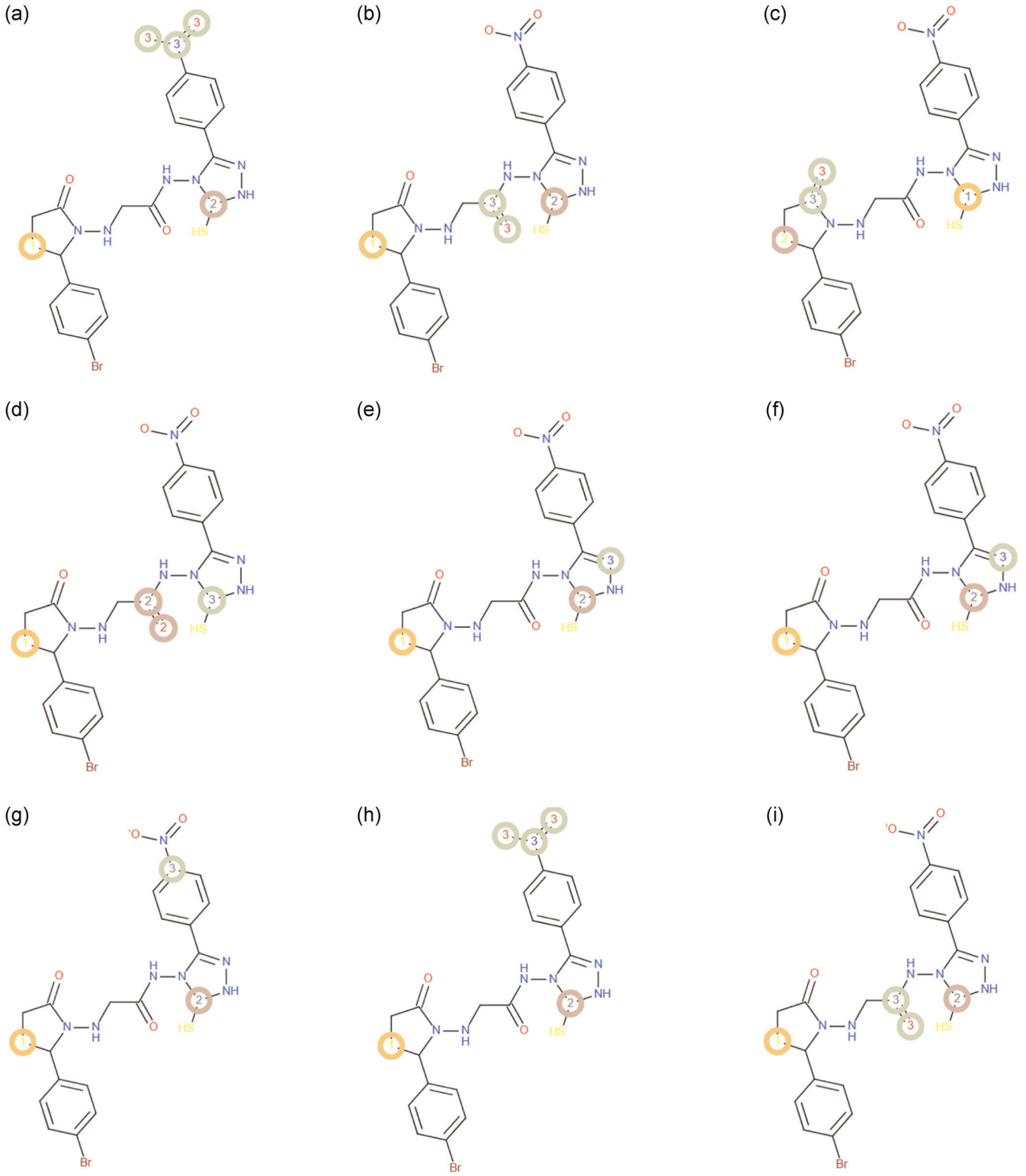

FIGURE 7 Prediction of the site of metabolism by RS-Predictor of compound **10b** at (a) CYP1A2, (b) CYP2A6, (c) CYP2B6, (d) CYP2C8, (e) CYP2C9, (f) CYP2C19, (g) CYP2D6, (h) CYP2E1, (i) CYP3A4. Color code: orange: highly labile; gray: moderately labile; and light green: fairly labile

2.8 | Fingerprinting and molecular similarity

The ChEMBL database holds manually curated bioactive molecules with drug-like properties. To check whether any similar molecules/scaffolds are under investigation as potential DNA gyrase inhibitors, a similarity search for newly synthesized hybrid compounds was performed against molecules from the ChEMBL database tested for DNA gyrase inhibition (from now on, referred to as ChEMBL

TABLE 3 Two-dimensional (2D) structures of synthesized compounds and selected FDA-approved drugs[a] with the lowest binding score for DNA gyrase (PDB ID: 2XCT)

Compound	2D structure	Score	Compound	2D	Score
10a	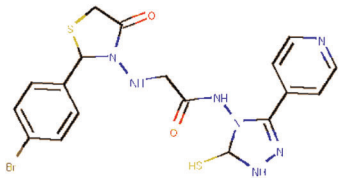	−10.1	10b	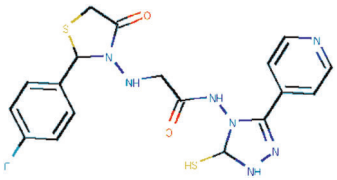	−10.2
10c	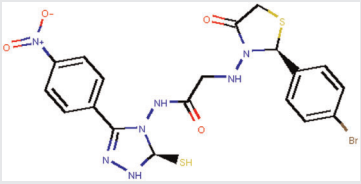	−9.8	10d	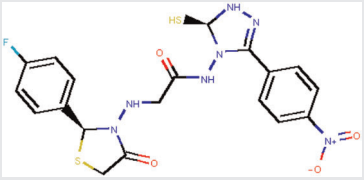	−9.4
10e	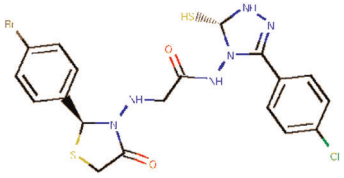	−9.9	10f	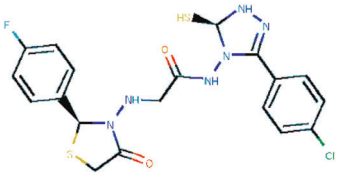	−9.7
10g	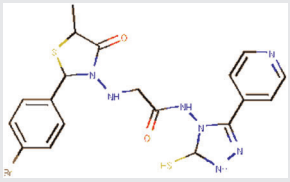	−8.3	10h	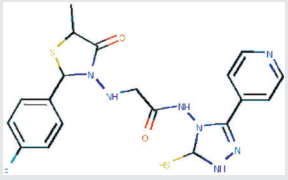	−9.7
10i	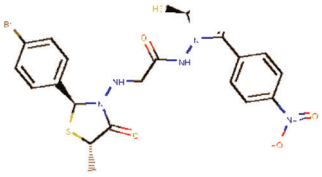	−9.2	10j	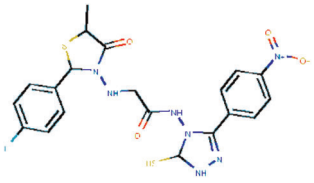	−8.8
10k	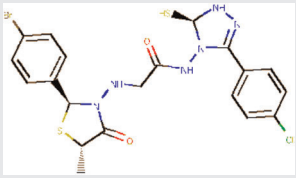	−9.7	10l	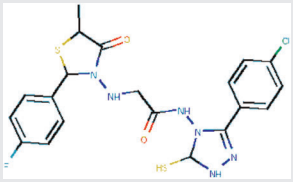	−9.4
10m	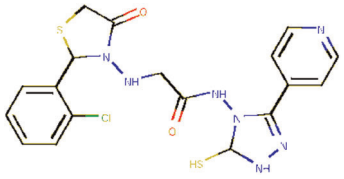	−9.6	10n	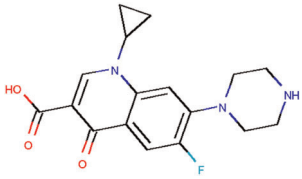	−10.2
10o	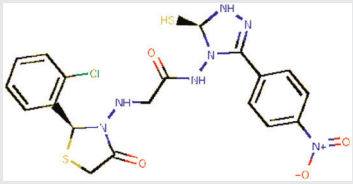	−10.1	10p	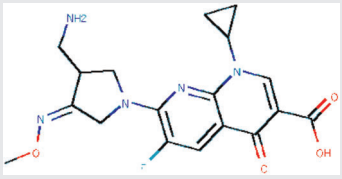	−9.6

TABLE 3 (Continued)

Compound	2D structure	Score	Compound	2D	Score
10q	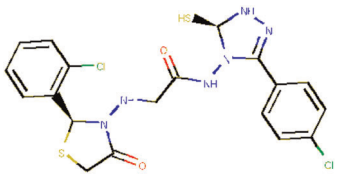	−10.2	**10r**		−10.0
CPF	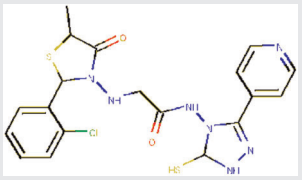	−9.6	GEM	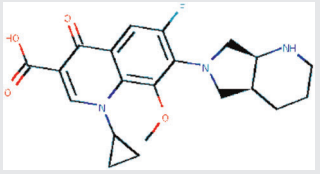	−9.9
LEV	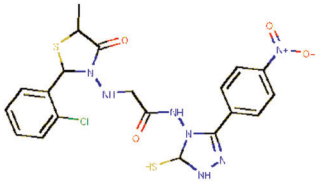	−10.0	MOX	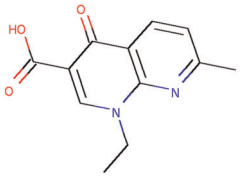	−10.2
NAL	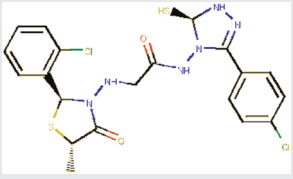	−7.9	NOR	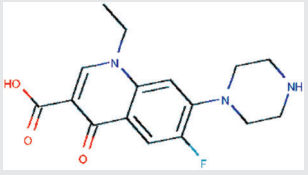	−9.1

[a]CPF, ciprofloxacin; GEM, gemifloxacin; LEV, levofloxacin; MOX, moxifloxacin; NAL, nalidixic acid; NOR, norfloxacin.

molecules). The molecular similarity was estimated on the basis of the similarity of 2D molecular fingerprints calculated using the extended connectivity fingerprint (FP) approach. The adopted method was demonstrated to have the highest precision on average, according to database search by compound similarity based on FP.[48] The molecular similarity between newly synthesized and ChEMBL molecules is presented as a heat map in Figure S4, with only those compounds that have Tanimoto's coefficient for at least one hybrid compound higher than 0.20. Three compounds (CHEMBL457095, CHEMBL458404, and CHEMBL458367) were found to have the highest Tanimoto molecular similarity index for the biggest subset of our molecules. CHEMBL457095 has T_C equal to 0.27, when compared with compound **10l**. It also enters the molecules most similar to hit compounds **10b** and **10n** to the top three compounds. The value by itself is relatively low, meaning that they have only some fragments in common, like halogen-substituted benzene ring, carbonyl group, or five-membered nitrogen-containing ring. Figure S5 displays the 2D structures of most similar molecoules of ChEMBL database and there Tanimoto's coefficient. For CHEMBL457095, the experimentally measured IC_{50} value for DNA gyrase inhibition is 0.5 μg/ml.[49] This is 50 times lower as compared with **10n**, corroborating that our compounds are members of the new class of potential DNA gyrase inhibitors, whose activity could be increased by targeted substitutions.

3 | CONCLUSION

Here, we report a synthesis of a series of hybrid 1,2,4-triazole and oxothiazolidin derivatives and their antibacterial activity. The SAR indicated that the introduction of electron-withdrawing groups such as halobenzene moiety into the 1,2,4-triazole ring increases ligand potency in DNA gyrase inhibition. In vitro antibacterial evaluation showed that compounds **10b** and **10n** have the potential to inhibit a variety of Gram-positive and -negative bacteria through additional mechanisms of action, such as modulating the DNA gyrase activity. In this regard, **10b** and **10n** are excellent lead compounds with efficiency similar to that of a series of FDA-approved drugs that act as DNA gyrase inhibitors. Experimental findings are corroborated by docking studies. Interaction pattern analysis revealed intercalation of aromatic groups between two subsequent DNA base pairs, in a similar fashion as the known DNA gyrase inhibitors ciprofloxacin, gemifloxacin, levofloxacin, moxifloxacin, and norfloxacin. The low molecular similarity compared with 430 compounds from ChEMBL, which were tested as DNA gyrase inhibitors, demonstrates that molecules with oxothiazolidin–1,2,4-triazole scaffolds are a novel class of potential DNA gyrase inhibitors. Their further investigation and targeted substitution might help us fight against resistant bacteria.

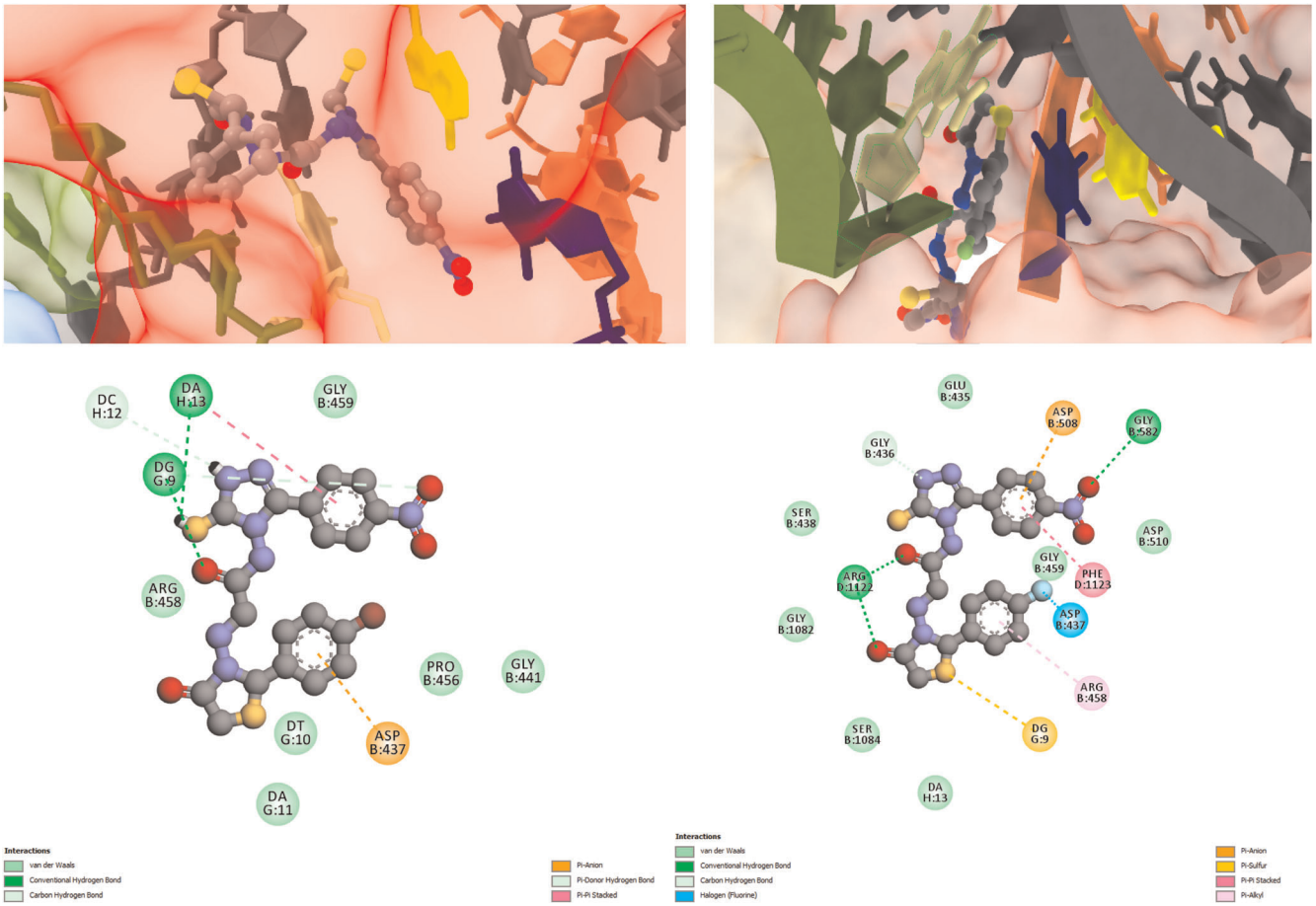

FIGURE 8 Insight into the catalytic site neighborhood of DNA gyrase (PDB ID: 2XCT) for the best poses and two-dimensional interaction of **10b** (left) and **10n** (right) obtained by docking

4 | EXPERIMENTAL

4.1 | Chemistry

4.1.1 | General

All experiments were carried out using commercial reagents and analytical grade solvents without further purification. Thin-layer chromatography (TLC) was performed on precoated silica gel plates (F254 grade, 0.2 mm thickness), using ethyl acetate/*n*-hexane (3:7) as an eluent, and visualization was carried out in an iodine chamber. The completion of the reaction and purity of the synthesized derivatives were evaluated on the basis of a sharp single spot. Melting points of the derivatives were determined using Veego (MPI melting point instrument). ^{1}H NMR and ^{13}C NMR analysis were performed using JEOL 300 and Bruker Avance II 100 NMR spectrometers, respectively, with $CDCl_3$ as the solvent and tetramethylsilane (TMS) as the internal standard. Mass spectra were obtained using the VG-AUTOSPEC spectrometer equipped with an ESI source (Fisons Instruments). Elemental analysis was carried out on a Vario EL-III CHNOS elemental analyzer (Elementar Analysensysteme).

The InChI codes of the investigated compounds, together with some biological activity data, are provided as Supporting Information.

4.1.2 | Synthesis of 1,2,4-triazoles (**5a–c**)

The derivatives **5a–c** were synthesized from the reagents **1a–c** as described in our previous study.[26]

4.1.3 | Synthesis of 2-chloro-*N*-(5-mercapto-3-substituted-phenyl-1,5-dihydro-4*H*-1,2,4-triazol-4-yl) (**6a–c**)

Here, 0.5 mol of substituted 1,2,4-triazoles **5a–c** was dissolved in the glacial acetic acid (25 ml), which contained 25 ml of a saturated solution of sodium acetate. If the substance did not dissolve completely, the mixture was heated to make the solution clear. The reaction mixture was cooled on an ice bath, and chloroacetyl chloride (0.06 mol, 5 ml) was added in a dropwise manner with continuous stirring to avoid vigorous proceeding of reaction. After 30–45 min, an

off-white product was formed, which was separated through simple filtration. Furthermore, the product was washed with 50% aqueous acetic acid, followed by distilled water and recrystallization from absolute alcohol.

4.1.4 | Synthesis of 2-hydrazinyl-*N*-(5-mercapto-3-substituted-phenyl-1,5-dihydro-4*H*-1,2,4-triazol-4-yl)-acetamides (**7a–c**)

Here, 0.01 mol of *N*-(5-aryl-1,2,4-triazole-2-yl)-2-chloroacetamides **6a–c** was dissolved in 25 ml of ethanol. Furthermore, 0.01 mol (5 ml) of hydrazine hydrate was added into the reaction mixture and the resultant mixture was poured on the crushed ice to separate the product.

4.1.5 | Synthesis of 2-[2-(substituted-phenyl)-5-substituted-4-oxo-thiazolidin-3-ylamino]-*N*-[5-mercapto-3-(substituted-phenyl)-1,5-dihydro-1,2,4-triazol-4-yl]acetamides (**10a–r**)

A mixture of 2-hydrazinyl-*N*-(5-mercapto-3-substituted-phenyl-1,5-dihydro-1,2,4-triazol-4-yl)acetamides (**7a–c**) (0.01 mol), substituted benzaldehydes (**8a–c**) (0.01 mol), thioglycolic acid derivatives (**9a–c**) (0.01 mol), and a pinch of $ZnCl_2$ were refluxed in 15 ml of ethanol for 6–7 h or reflux until a distinct single point was obtained on TLC. As a result of the reaction, a solid was formed and separated on the bottom of the vessel. Furthermore, the products were filtered, washed with water, and recrystallized with ethanol to obtain the pure compound.

*2-{[2-(4-Bromophenyl)-4-oxothiazolidin-3-yl]amino}-*N*-[5-mercapto-3-(pyridin-4-yl)-1,5-dihydro-4*H*-1,2,4-triazol-4-yl]acetamide (**10a**)*

Yellow solid; yield: 78%; molecular formula: $C_{18}H_{18}BrN_7O_2S_2$; melting point: 251–253°C; molecular weight: 508.41; ^{1}H NMR (300 MHz, $CDCl_3$, TMS) δ ppm: 1.524 (s, 1H, SH), 3.612–3.562 (d, 1H, J = 15.0 Hz, CH_2, thiazolidine), 3.802–3.762 (d, 1H, J = 12.0 Hz, CH_2, thiazolidine), 3.943 (s, 2H, CH_2), 4.243 (s, 1H, NH), 6.296 (s, 1H, CH, thiazolidine), 6.426 (s, 1H, CH, triazole), 7.16–7.135 (d, 2H, J = 7.5 Hz, Br–Ph), 7.572–7.558 (d, 2H, J = 4.2 Hz, CH, pyridine), 7.630–7.604 (d, 2H, J = 7.8 Hz, Br–Ph), 8.679–8.664 (d, 2H, J = 4.5 Hz, CH, pyridine), 8.876 (s, 1H, NH), 9.134 (s, 1H, NH); ^{13}C NMR (100 MHz, $CDCl_3$) δ ppm: 33.89, 49.27, 66.24, 72.5, 121.33, 124.02, 126.8, 127.82, 130.95, 136.95, 145.2, 149.65, 165.8, 167.26; MS-ESI (m/z): 508.25 $[M+H]^+$; elemental analysis: calculated C: 42.52%, H: 3.57%, N: 19.29%; found C: 42.40%, H: 3.42%, N: 19.65%.

*2-{[2-(4-Bromophenyl)-4-oxothiazolidin-3-yl]amino}-*N*-[5-mercapto-3-(4-nitrophenyl)-1,5-dihydro-4*H*-1,2,4-triazol-4-yl]acetamide (**10b**)*

Yellow-brown solid; yield: 76%; molecular formula: $C_{19}H_{18}BrN_7O_4S_2$; melting point: 184–186°C; molecular weight: 552.42; ^{1}H NMR (300 MHz, $CDCl_3$, TMS) δ ppm: 1.524 (s, 1H, SH), 3.602–3.562 (d, 1H, J = 12.0 Hz, CH_2, thiazolidine), 3.802–3.762 (d, 1H, J = 12.0 Hz, CH_2, thiazolidine), 3.943 (s, 2H, CH_2), 4.243 (s, 1H, NH), 6.302 (s, 1H, CH, thiazolidine), 6.463 (s, 1H, CH, triazole), 7.14–7.115 (d, 2H, J = 7.5 Hz, Br–Ph), 7.682–7.652 (d, 2H, J = 9.0 Hz, NO_2–Ph), 7.630–7.604 (d, 2H, J = 7.8 Hz, Br–Ph), 8.121–8.092 (d, 2H, J = 8.7 Hz, NO_2–Ph), 8.876 (s, 1H, NH), 9.134 (s, 1H, NH); ^{13}C NMR (100 MHz, $CDCl_3$) δ ppm: 33.89, 49.27, 66.24, 72.2, 124.02, 126.2, 127.85, 128.13, 129.65, 130.95, 136.95, 145.2, 147.98, 165.8, 167.26; MS-ESI (m/z): 551.10 $[M+H]^+$; elemental analysis: calculated C: 41.315%, H: 3.28%, N: 17.75%; found C: 41.40%, H: 3.42%, N: 17.65%.

*2-{[2-(4-Bromophenyl)-4-oxothiazolidin-3-yl]amino}-*N*-[3-(4-chlorophenyl)-5-mercapto-1,5-dihydro-4*H*-1,2,4-triazol-4-yl]-acetamide (**10c**)*

Light yellow solid; yield: 80%; molecular formula: $C_{19}H_{18}BrClN_6O_2S_2$; melting point: 253–255°C; molecular weight: 541.87; ^{1}H NMR (300 MHz, $CDCl_3$, TMS) δ ppm: 1.524 (s, 1H, SH), 3.602–3.562 (d, 1H, J = 12.0 Hz, CH_2, thiazolidine), 3.802–3.762 (d, 1H, J = 12.0 Hz, CH_2, thiazolidine), 3.493 (s, 2H, CH_2), 4.243 (s, 1H, NH), 6.296 (s, 1H, CH, thiazolidine), 6.463 (s, 1H, CH, triazole), 7.16–7.135 (d, 2H, J = 7.5 Hz, Br–Ph), 7.635–7.611 (d, 2H, J = 7.2 Hz, Br–Ph), 7.674–7.649 (d, 2H, J = 7.5 Hz, Cl–Ph), 7.921–7.892 (d, 2H, J = 8.7 Hz, Cl–Ph), 8.876 (s, 1H, NH), 9.134 (s, 1H, NH); ^{13}C NMR (100 MHz, $CDCl_3$) δ ppm: 33.89, 49.27, 66.24, 72.7, 124.02, 126.2, 127.82, 128.09, 129.08, 130.95, 135.68, 136.95, 145.2, 165.8, 167.26; MS-ESI (m/z): 540.12 $[M+H]^+$; elemental analysis: calculated C: 42.12%, H: 3.35%, N: 15.51%; found C: 42.20%, H: 3.42%, N: 15.62%.

*2-{[2-(4-Bromophenyl)-5-methyl-4-oxothiazolidin-3-yl]amino}-*N*-[5-mercapto-3-(pyridin-4-yl)-1,5-dihydro-4*H*-1,2,4-triazol-4-yl]-acetamide (**10d**)*

Yellow solid; yield: 74%; molecular formula: $C_{19}H_{20}BrN_7O_2S_2$; melting point: 193–195°C; molecular weight: 522.44; ^{1}H NMR (300 MHz, $CDCl_3$, TMS) δ ppm: 1.264–1.241 (d, 3H, J = 6.9 Hz, CH_3), 1.524 (s, 1H, SH), 3.493 (s, 2H, CH_2), 4.092 (m, 1H, CH, thiazolidine), 4.243 (s, 1H, NH), 6.216 (s, 1H, CH, thiazolidine), 6.423 (s, 1H, CH, triazole), 7.16–7.135 (d, 2H, J = 7.5 Hz, Br–Ph), 7.630–7.604 (d, 2H, J = 7.8 Hz, Br–Ph), 7.664–7.649 (d, J = 4.5 Hz, CH, pyridine), 8.664–8.679 (d, 2H, J = 4.5 Hz, CH, pyridine), 8.876 (s, 1H, NH), 9.134 (s, 1H, NH); ^{13}C NMR (100 MHz, $CDCl_3$) δ ppm: 33.89, 49.27, 66.24, 72.75, 121.33, 124.02, 126.80, 127.82, 127.82, 130.95, 136.95, 145.2, 149.65, 165.8, 167.26; MS-ESI (m/z): 521.32 $[M+H]^+$; elemental analysis: calculated C: 43.68%, H: 3.86%, N: 18.77%; found C: 43.45%, H: 3.82%, N: 18.72%.

*2-{[2-(4-Bromophenyl)-5-methyl-4-oxothiazolidin-3-yl]amino}-*N*-[5-mercapto-3-(4-nitrophenyl)-1,5-dihydro-4*H*-1,2,4-triazol-4-yl]-acetamide (**10e**)*

Yellow-brown solid; yield: 72%; molecular formula: $C_{20}H_{20}BrN_7O_4S_2$; melting point: 213–215°C; molecular weight: 566.45; ^{1}H NMR (300 MHz, $CDCl_3$, TMS) δ ppm: 1.264–1.241 (d, 3H, J = 6.9 Hz, CH_3), 1.524 (s, 1H, SH), 3.953 (s, 2H, CH_2), 4.092 (m, 1H, J = 7.0 Hz, CH, thiazolidine), 4.243 (s, 1H, NH), 6.423 (1H, s, CH, triazole), 7.16–7.135 (d, 2H, J = 7.5 Hz, Br–Ph), 7.682–7.652 (d, 2H, J = 9.0 Hz,

NO_2–Ph), 7.630–7.604 (d, 2H, *J* = 7.8 Hz, Br–Ph), 8.121–8.092 (d, 2H, *J* = 8.7 Hz, NO_2–Ph), 8.876 (s, 1H, NH), 9.134 (s, 1H, NH); ^{13}C NMR (100 MHz, $CDCl_3$) *δ* ppm: 17.8, 44.31, 49.27, 66.24, 72.75, 117.29, 124.02, 126.2, 127.82, 128.1, 130.95, 136.95, 140.47, 145.2, 165.8, 167.26; MS-ESI (*m/z*): 565.52 $[M+H]^+$; elemental analysis: calculated C: 42.41%, H: 3.56%, N: 17.31%; found C: 42.5%, H: 3.75%, N: 17.52%.

*2-{[2-(4-Bromophenyl)-5-methyl-4-oxothiazolidin-3-yl]amino}-*N*-[3-(4-chlorophenyl)-5-mercapto-1,5-dihydro-4*H*-1,2,4-triazol-4-yl]-acetamide (**10f**)*

Yellow solid; yield: 76%; molecular formula: $C_{20}H_{20}BrClN_6O_2S_2$; melting point: 241–243°C; molecular weight: 555.89; ^{1}H NMR (300 MHz, $CDCl_3$, TMS) *δ* ppm: 1.264–1.241 (d, 3H, *J* = 6.9 Hz, CH_3), 1.524 (s, 1H, SH), 3.953 (s, 2H, CH_2), 4.092 (m, 1H, *J* = 7.0 Hz, CH, thiazolidine), 4.243 (s, 1H, NH), 6.296 (1H, s, CH, thiazolidine), 6.463 (s, 1H, CH, triazole), 7.16–7.135 (d, 2H, *J* = 7.5 Hz, Br–Ph), 7.630–7.605 (d, 2H, *J* = 7.5 Hz, Br–Ph), 7.674–7.648 (d, 2H, *J* = 7.8 Hz, Cl–Ph), 7.921–7.892 (d, 2H, *J* = 8.7 Hz, Cl–Ph), 8.876 (s, 1H, NH), 9.134 (s, 1H, NH); ^{13}C NMR (100 MHz, $CDCl_3$) *δ* ppm: 17.8, 44.31, 49.27, 66.24, 72.5, 117.29, 124.02, 126.2, 127.82, 128.52, 130.95, 136.95, 140.47, 145.2, 165.8, 167.26; MS-ESI (*m/z*): 554.10 $[M+H]^+$; elemental analysis: calculated C: 43.21%, H: 3.63%, N: 15.12%; found C: 43.4%, H: 3.52%, N: 15.24%.

*2-{[2-(2-Chlorophenyl)-4-oxothiazolidin-3-yl]amino}-*N*-[5-mercapto-3-(pyridin-4-yl)-1,5-dihydro-4*H*-1,2,4-triazol-4-yl]acetamide (**10g**)*

Brown solid; yield: 71%; molecular formula: $C_{18}H_{18}ClN_7O_2S_2$; melting point: 176–178°C; molecular weight: 463.96; ^{1}H NMR (300 MHz, $CDCl_3$, TMS) *δ* ppm: 1.524 (s, 1H, –SH), 3.602–3.562 (d, 1H, *J* = 12.0 Hz, CH_2, thiazolidine), 3.802–3.762 (d, 1H, *J* = 12.0 Hz, CH_2, thiazolidine), 3.953 (s, 2H, CH_2), 4.243 (s, 1H, NH), 6.296 (s, 1H, CH, thiazolidine), 6.463 (s, 1H, CH, triazole), 7.215 (m, 1H, Ph–Cl), 7.334 (m, 1H, Ph–Cl), 7.524 (m, 1H, Cl–Ph), 7.664–7.651 (d, 2H, *J* = 3.9 Hz, CH, pyridine), 7.921–7.892 (d, 2H, *J* = 8.7 Hz, Cl–Ph), 8.679–8.664 (d, 2H, *J* = 4.5 Hz, CH, pyridine), 8.876 (s, 1H, NH), 9.134 (s, 1H, NH); ^{13}C NMR (100 MHz, $CDCl_3$) *δ* ppm: 33.89, 49.27, 66.24, 72.15, 121.33, 126.8, 127.82, 128.71, 130.66, 133.16, 134.10, 136.92, 145.2, 149.65, 165.8, 167.26; MS-ESI (*m/z*): 463.42 $[M+H]^+$; elemental analysis: calculated C: 46.60%, H: 3.91%, N: 21.13%; found C: 46.25%, H: 3.92%, N: 21.2%.

*2-{[2-(2-Chlorophenyl)-4-oxothiazolidin-3-yl]amino}-*N*-[5-mercapto-3-(4-nitrophenyl)-1,5-dihydro-4*H*-1,2,4-triazol-4-yl]acetamide (**10h**)*

Yellow solid; yield: 74%; molecular formula: $C_{19}H_{18}ClN_7O_4S_2$; melting point: 255°C; molecular weight: 507.97; ^{1}H NMR (300 MHz, $CDCl_3$, TMS) *δ* ppm: 1.524 (s, 1H, SH), 3.602–3.562 (d, 1H, *J* = 12.0 Hz, CH_2, thiazolidine), 3.802–3.762 (d, 1H, *J* = 12.0 Hz, CH_2, thiazolidine), 3.953 (s, 2H, CH_2), 6.296 (s, 1H, CH, thiazolidine), 4.243 (s, 1H, NH), 6.463 (s, 1H, CH, triazole), 7.215 (m, 1H, Ph–Cl), 7.334 (m, 1H, Ph–Cl), 7.524 (m, 1H, Cl–Ph), 7.921–7.892 (d, 2H, *J* = 8.7 Hz, Cl–Ph), 8.12–8.092 (d, 2H, *J* = 8.4 Hz, NO_2–Ph), 8.489–8.462 (d, 2H, *J* = 8.1 Hz, CH, NO_2–Ph), 8.872 (s, 1H, NH), 9.132 (s, 1H, NH); ^{13}C NMR (100 MHz, $CDCl_3$) *δ* ppm: 33.89, 49.27, 66.24, 72.7, 123.98, 126.2, 127.82, 128.71, 130.66, 133.16, 134.10, 136.92, 145.2, 147.98, 149.65, 165.8, 167.26; MS-ESI (*m/z*): 507.45 $[M+H]^+$; elemental analysis: calculated C: 44.93%, H: 3.57%, N: 19.30%; found C: 44.5%, H: 3.42%, N: 19.75%.

*2-{[2-(2-Chlorophenyl)-4-oxothiazolidin-3-yl]amino}-*N*-[3-(4-chlorophenyl)-5-mercapto-1,5-dihydro-4*H*-1,2,4-triazol-4-yl]-acetamide (**10i**)*

White solid; yield: 76%; molecular formula: $C_{19}H_{18}Cl_2N_6O_2S_2$; melting point: 241–243°C; molecular weight: 497.41; ^{1}H NMR (300 MHz, $CDCl_3$, TMS) *δ* ppm: 1.524 (s, 1H, SH), 3.602–3.562 (d, 1H, *J* = 12.0 Hz, CH_2, thiazolidine), 3.802–3.762 (d, 1H, *J* = 12.0 Hz, CH_2, thiazolidine), 3.953 (s, 2H, CH_2), 6.296 (s, 1H, CH, thiazolidine), 4.243 (s, 1H, NH), 6.463 (s, 1H, CH, triazole), 7.215 (m, 1H, Ph–Cl), 7.334 (m, 1H, Ph–Cl), 7.398–7.373 (d, 2H, *J* = 7.5 Hz, Cl–Ph), 7.425–7.41 (d, 2H, *J* = 7.5 Hz, Cl–Ph), 7.524 (m, 1H, Cl–Ph), 7.921–7.892 (d, 2H, *J* = 8.7 Hz, Cl–Ph), 8.872 (s, 1H, NH), 9.132 (s, 1H, NH); ^{13}C NMR (100 MHz, $CDCl_3$) *δ* ppm: 33.89, 49.27, 66.24, 72.7, 126.2, 127.82, 128.09, 128.71, 129.08, 130.66, 133.16, 135.68, 136.92, 145.2, 149.62, 165.8, 167.26; MS-ESI (*m/z*): 496.52 $[M+H]^+$; elemental analysis: calculated C: 45.88%, H: 3.65%, N: 16.90%; found C: 45.58%, H: 3.78%, N: 16.70%.

*2-{[2-(2-Chlorophenyl)-5-methyl-4-oxothiazolidin-3-yl]amino}-*N*-[5-mercapto-3-(pyridin-4-yl)-1,5-dihydro-4*H*-1,2,4-triazol-4-yl]-acetamide (**10j**)*

Reddish-yellow solid; yield: 72%; molecular formula: $C_{19}H_{20}ClN_7O_2S_2$; melting point: 243–245°C; molecular weight: 477.99; ^{1}H NMR (300 MHz, $CDCl_3$, TMS) *δ* ppm: 1.241–1.264 (d, 3H, *J* = 7.0 Hz, CH_3), 1.524 (s, 1H, SH), 3.953 (s, 2H, CH_2), 4.092 (m, 1H, CH, thiazolidine), 4.243 (s, 1H, NH), 6.213 (s, 1H, CH, triazole), 6.296 (s, 1H, CH, thiazolidine), 6.463 (s, 1H, CH, triazole), 7.215–7.19 (m, 1H, Ph–Cl), 7.334–7.303 (m, 1H, Ph–Cl), 7.524 (m, 1H, Cl–Ph), 7.664–7.649 (d, 2H, *J* = 4.5 Hz, CH, pyridine), 7.921–7.892 (d, 2H, *J* = 8.7 Hz, Cl–Ph), 8.679–8.664 (d, 2H, *J* = 4.5 Hz, CH, pyridine), 8.876 (s, 1H, NH), 9.134 (s, 1H, NH); ^{13}C NMR (100 MHz, $CDCl_3$) *δ* ppm: 17.8, 44.31, 49.27, 66.24, 72.7, 121.33, 122.2, 126.80, 127.82, 128.71, 130.66, 133.16, 136.92, 145.2, 149.65, 165.8, 167.26; MS-ESI (*m/z*): 477.82 $[M+H]^+$; elemental analysis: calculated C: 47.74%, H: 4.22%, N: 20.51%; found C: 47.8%, H: 4.28%, N: 20.42%.

*2-{[2-(2-Chlorophenyl)-5-methyl-4-oxothiazolidin-3-yl]amino}-*N*-[5-mercapto-3-(4-nitrophenyl)-1,5-dihydro-4*H*-1,2,4-triazol-4-yl]-acetamide (**10k**)*

Brown solid; yield: 79%; molecular formula: $C_{20}H_{20}ClN_7O_4S_2$; melting point: 237–235°C; molecular weight: 522; ^{1}H NMR (300 MHz, $CDCl_3$, TMS) *δ* ppm: 1.241–1.264 (d, 3H, *J* = 7.0 Hz, CH_3), 1.524 (s, 1H, SH), 3.953 (s, 2H, CH_2), 4.092 (m, 1H, CH, thiazolidine), 4.243 (s, 1H, NH), 6.296 (s, 1H, CH, thiazolidine), 6.463 (s, 1H, CH, triazole), 7.215 (m, 1H, Ph–Cl), 7.334 (m, 1H, Ph–Cl), 7.524 (m, 1H, Cl–Ph), 7.921–7.892 (d, 2H, *J* = 8.7 Hz, Cl–Ph), 8.12–8.092 (d, 2H, *J* = 8.4 Hz, NO_2–Ph), 8.489–8.462 (d, 2H, *J* = 8.1 Hz, CH, NO_2–Ph), 8.872 (s, 1H,

NH), 9.132 (s, 1H, NH); ^{13}C NMR (100 MHz, $CDCl_3$) δ ppm: 17.8, 44.31, 49.27, 66.24, 72.2, 121.33, 122.2, 123.98, 126.2, 127.58, 128.13, 128.92, 130.55, 133.16, 145.2, 147.98, 165.8, 167.26; MS-ESI (*m/z*): 521.2 $[M+H]^+$; elemental analysis: calculated C: 46.02%, H: 3.86%, N: 18.78%; found C: 46.25%, H: 3.92%, N: 18.85%.

N-*[3-(4-Chlorophenyl)-5-mercapto-1,5-dihydro-4*H*-1,2,4-triazol-4-yl]-2-{[2-(2-chlorophenyl)-5-methyl-4-oxothiazolidin-3-yl]amino}-acetamide (**10l**)*

Yellow solid; yield: 68%; molecular formula: $C_{20}H_{20}Cl_2N_6O_2S_2$; melting point: 167°C; molecular weight: 511.44; ^{1}H NMR (300 MHz, $CDCl_3$, TMS) δ ppm: 1.241–1.264 (d, 3H, J = 7.0 Hz, CH_3), 1.524 (s, 1H, SH), 3.953 (s, 2H, CH_2), 4.092 (m, 1H, CH, thiazolidine), 4.243 (s, 1H, NH), 6.296 (s, 1H, CH, thiazolidine), 6.463 (s, 1H, CH, triazole), 7.215 (m, 1H, Ph–Cl), 7.334 (m, 1H, Ph–Cl), 7.398–7.373 (d, 2H, J = 7.5 Hz, Cl–Ph), 7.425–7.392 (d, 2H, J = 8.4 Hz, Cl–Ph), 7.524 (m, 1H, Cl–Ph), 7.921–7.892 (d, 2H, J = 8.7 Hz, Cl–Ph), 8.872 (s, 1H, NH), 9.132 (s, 1H, NH); ^{13}C NMR (100 MHz, $CDCl_3$) δ ppm: 17.8, 44.31, 49.27, 66.24, 72.2, 121.33, 122.2 126.2, 127.82, 128.15, 128.71, 129.08, 130.66, 133.16, 135.68, 145.2, 165.8, 167.26; MS-ESI (*m/z*): 510.2 $[M+H]^+$; elemental analysis: calculated C: 46.97%, H: 3.94%, N: 16.43%; found C: 46.90%, H: 3.8%, N: 16.75%.

*2-{[2-(4-Fluorophenyl)-4-oxothiazolidin-3-yl}amino]-*N*-[5-mercapto-3-(pyridin-4-yl)-1,5-dihydro-4*H*-1,2,4-triazol-4-yl]acetamide (**10m**)*

Yellow solid; yield: 75%; molecular formula: $C_{18}H_{18}FN_7O_2S_2$; melting point: 171–173°C; molecular weight: 447.51; ^{1}H NMR (300 MHz, $CDCl_3$, TMS) δ ppm: 1.524 (s, 1H, SH), 3.612–3.562 (d, 1H, J = 15.0 Hz, CH_2, thiazolidine), 3.802–3.762 (d, 1H, J = 12.0 Hz, CH_2, thiazolidine), 3.943 (s, 2H, CH_2), 4.243 (s, 1H, NH), 6.296 (s, 1H, CH, thiazolidine), 6.426 (s, 1H, CH, triazole), 7.162–7.134 (d, 2H, J = 8.4 Hz, F–Ph), 7.572–7.561 (d, 2H, J = 3.3 Hz, CH, pyridine), 7.620–7.592 (d, 2H, J = 8.6 Hz, F–Ph), 8.664–8.679 (d, 2H, J = 4.5 Hz, CH, pyridine), 8.876 (s, 1H, NH), 9.134 (s, 1H, NH); ^{13}C NMR (100 MHz, $CDCl_3$) δ ppm: 33.89, 49.27, 66.24, 72.2, 115.16, 121.33, 126.8, 127.82, 136.95, 145.2, 149.65, 163.35, 165.8, 167.26; MS-ESI (*m/z*): 447.12 $[M+H]^+$; elemental analysis: calculated C: 48.31%, H: 4.05%, N: 21.91%; found C: 48.25%, H: 4.22%, N: 21.85%.

*2-{[2-(4-Fluorophenyl)-4-oxothiazolidin-3-yl]amino}-*N*-[5-mercapto-3-(4-nitrophenyl)-1,5-dihydro-4*H*-1,2,4-triazol-4-yl]acetamide (**10n**)*

Yellow-brown solid; yield: 71%; molecular formula: $C_{19}H_{18}FN_7O_4S_2$; melting point: 260–262°C; molecular weight: 491.52; ^{1}H NMR (300 MHz, $CDCl_3$, TMS) δ ppm: 1.524 (s, 1H, SH), 3.612–3.562 (d, 1H, J = 15.0 Hz, CH_2, thiazolidine), 3.802–3.762 (d, 1H, J = 12.0 Hz, CH_2, thiazolidine), 3.943 (s, 2H, CH_2), 4.243 (s, 1H, NH), 6.296 (s, 1H, CH, thiazolidine), 6.426 (s, 1H, CH, triazole), 7.162–7.134 (d, 2H, J = 8.4 Hz, F–Ph), 7.620–7.591 (d, 2H, J = 8.6 Hz, F–Ph), 7.662–7.6336 (d, 2H, J = 8.5 Hz, NO_2–Ph), 8.121–8.092 (d, 2H, J = 8.7 Hz, NO_2–Ph), 8.876 (s, 1H, NH), 9.134 (s, 1H, NH); ^{13}C NMR (100 MHz, $CDCl_3$) δ ppm: 33.89, 49.27, 66.24, 72.2, 115.16, 123.98, 126.2, 127.82, 128.13, 136.95, 145.2, 147.98, 163.35, 165.8, 167.26; MS-ESI (*m/z*): 491.25 $[M+H]^+$; elemental analysis: calculated C: 46.43%, H: 3.69%, N: 19.95%; found C: 46.52%, H: 3.25%, N: 19.75%.

N-*[3-(4-Chlorophenyl)-5-mercapto-1,5-dihydro-4*H*-1,2,4-triazol-4-yl]-2-{[2-(4-fluorophenyl)-4-oxothiazolidin-3-yl]amino}-acetamide (**10o**)*

Brown solid; yield: 77%; molecular formula: $C_{19}H_{18}ClFN_6O_2S_2$; melting point: 231–233°C; molecular weight: 480.96; ^{1}H NMR (300 MHz, $CDCl_3$, TMS) δ ppm: 1.524 (s, 1H, SH), 3.612–3.562 (d, 1H, J = 15.0 Hz, CH_2, thiazolidine), 3.802–3.762 (d, 1H, J = 12.0 Hz, CH_2, thiazolidine), 3.943 (s, 2H, CH_2), 4.243 (s, 1H, NH), 6.296 (s, 1H, CH, thiazolidine), 6.426 (s, 1H, CH, triazole), 7.162–7.134 (d, 2H, J = 8.4 Hz, F–Ph), 7.398–7.373 (d, 2H, J = 7.5 Hz, Cl–Ph), 7.425–7.4 (d, 2H, J = 7.5 Hz, Cl–Ph), 7.620–7.591 (d, 2H, J = 8.6 Hz, F–Ph), 8.876 (s, 1H, NH), 9.134 (s, 1H, NH); ^{13}C NMR (100 MHz, $CDCl_3$) δ ppm: 33.89, 49.27, 66.24, 72.2, 115.16, 126.2, 127.82, 128.09, 129.08, 135.68, 136.95, 145.2, 163.35, 165.8, 167.22; MS-ESI (*m/z*): 480.25 $[M+H]^+$; elemental analysis: calculated C: 47.45%, H: 3.77%, N: 17.47%; found C: 47.5%, H: 3.95%, N: 17.56%.

*2-{[2-(4-Fluorophenyl)-5-methyl-4-oxothiazolidin-3-yl]amino}-*N*-[5-mercapto-3-(pyridin-4-yl)-1,5-dihydro-4*H*-1,2,4-triazol-4-yl]-acetamide (**10p**)*

Yellow solid; yield: 73%; molecular formula: $C_{18}H_{18}FN_7O_2S_2$; melting point: 234–236°C; molecular weight: 447.51; ^{1}H NMR (300 MHz, $CDCl_3$, TMS) δ ppm: 1.241–1.264 (d, 3H, J = 7.0 Hz, CH_3), 1.524 (s, 1H, SH), 3.943 (s, 2H, CH_2), 4.092 (m, 1H, CH, thiazolidine), 4.243 (s, 1H, NH), 6.296 (s, 1H, CH, thiazolidine), 6.426 (s, 1H, CH, triazole), 7.572–7.557 (d, 2H, J = 4.5 Hz, CH, pyridine), 7.620–7.591 (d, 2H, J = 8.6 Hz, F–Ph), 8.664–8.679 (d, 2H, J = 4.5 Hz, CH, pyridine), 8.876 (s, 1H, NH), 9.134 (s, 1H, NH); ^{13}C NMR (100 MHz, $CDCl_3$) δ ppm: 17.8, 44.31, 49.27, 66.24, 72.2, 115.16, 121.33, 126.80, 127.82, 136.95, 145.2, 149.65, 163.35, 165.8, 167.26; MS-ESI (*m/z*): 447.52 $[M+H]^+$; elemental analysis: calculated C: 48.31%, H: 4.05%, N: 21.91%; found C: 48.15%, H: 3.98%, N: 21.75%.

*2-{[2-(4-Fluorophenyl)-5-methyl-4-oxothiazolidin-3-yl]amino}-*N*-[5-mercapto-3-(4-nitrophenyl)-1,5-dihydro-4*H*-1,2,4-triazol-4-yl]-acetamide (**10q**)*

Yellow solid; yield: 69%; molecular formula: $C_{20}H_{20}FN_7O_4S_2$; melting point: 232–234°C; molecular weight: 505.54; ^{1}H NMR (300 MHz, $CDCl_3$, TMS) δ ppm: 1.241–1.264 (d, 3H, J = 7.0 Hz, CH_3), 1.524 (s, 1H, SH), 3.943 (s, 2H, CH_2), 4.092 (m, 1H, J = 7.0 Hz, CH, thiazolidine), 3.943 (s, 2H, CH_2), 4.243 (s, 1H, NH), 6.296 (s, 1H, CH, thiazolidine), 6.426 (s, 1H, CH, triazole), 7.162–7.134 (d, 2H, J = 8.4 Hz, F–Ph), 7.620–7.591 (d, 2H, J = 8.6 Hz, F–Ph), 7.662–7.633 (d, 2H, J = 8.5 Hz, NO_2–Ph), 8.121–8.092 (d, 2H, J = 8.7 Hz, NO_2–Ph), 8.876 (s, 1H, NH), 9.134 (s, 1H, NH); ^{13}C NMR (100 MHz, $CDCl_3$) δ ppm: 17.8, 44.31, 49.27, 66.24, 72.2, 115.16, 123.98, 126.2, 127.82, 128.13, 136.95, 145.2, 147.98, 163.35, 165.8, 167.26; MS-ESI (*m/z*): 505.62 $[M+H]^+$; elemental analysis: calculated C: 47.52%, H: 3.99%, N: 19.39%; found C: 47.85%, H: 3.92%, N: 19.45%.

*N-[3-(4-Chlorophenyl)-5-mercapto-1,5-dihydro-4H-1,2,4-triazol-4-yl]-2-{[2-(4-fluorophenyl)-5-methyl-4-oxothiazolidin-3-yl]amino}-acetamide (**10r**)*

Brown solid; yield: 72%; molecular formula: $C_{20}H_{20}ClFN_6O_2S_2$; melting point: 189–191°C; molecular weight: 494.99; ^{1}H NMR (300 MHz, $CDCl_3$, TMS) δ ppm: 1.524 (s, 1H, SH), 3.943 (s, 2H, CH_2), 4.092 (m, 1H, J = 7.0 Hz, CH, thiazolidine), 3.943 (s, 2H, CH_2), 4.243 (s, 1H, NH), 6.296 (s, 1H, CH, thiazolidine), 6.426 (s, 1H, CH, triazole), 7.162–7.134 (d, 2H, J = 8.4 Hz, F–Ph), 7.398–7.373 (d, 2H, J = 7.5 Hz, Cl–Ph), 7.425–7.40 (d, 2H, J = 7.5 Hz, Cl–Ph), 7.620–7.591 (d, 2H, J = 8.6 Hz, F–Ph), 8.876 (s, 1H, NH), 9.134 (s, 1H, NH); ^{13}C NMR (100 MHz, $CDCl_3$) δ ppm: 17.8, 44.31, 49.27, 66.24, 72.2, 115.16, 126.2, 127.82, 128.09, 129.08, 135.68, 136.95, 145.2, 163.35, 165.8, 167.26; MS-ESI (m/z): 494.24 $[M+H]^+$; elemental analysis: calculated C: 48.53%, H: 4.07%, N: 16.98%; found C: 48.35%, H: 3.98%, N: 16.75%.

4.2 | Antibacterial activity

The antimicrobial potency of newly synthesized hybrid triazole derivatives was screened and expressed as MIC (μg/ml) against three Gram-positive (*B. subtilis* [NCIM 2063], *B. cereus* [NCIM 2156], *S. aureus* [NCIM 2079]), and two Gram-negative (*E. coli* [NCIM 2065] and *P. vulgaris* [NCIM 2027]) bacterial strains using the broth dilution method. Ciprofloxacin, a covalent DNA gyrase inhibitor, was used as the standard to perform the comparison of efficacy between the synthesized derivatives and standard antibacterial agent. Clinical and Laboratory Standards Institute methodology with a minor modification was used for the antibacterial activity evaluation.[50] Different concentrations of the test samples and standard compounds were prepared according to our previous research.[51,52]

4.3 | Antibiofilm activity

The potential of the hybrid thiazolidine–1,2,4-triazole derivatives to prevent initial cell attachment was investigated through the biofilm inhibition assay.[53] The bacterial strain of *S. aureus* (NCIM 2079) was cultured overnight in tryptone soya broth (supplemented with 0.5% glucose). Furthermore, different concentrations of test derivatives and standard ciprofloxacin (100 μl, ranging from 0 to 100 μg/ml) were mixed with the predefined bacterial suspension (having 100-μl aliquot of standardized concentration of cultures with OD_{560} = 0.02, 1.0×10^6 CFU/ml for each well and incubated at 37°C for 4 h without shaking) and then incubated for 24 h at 37°C under sterile condition.[54,55] After the completion of the incubation period, the culture medium was discarded and washed with phosphate-buffered saline to remove nonadherent bacteria. Now, each well of the microtiter plate was stained with 0.1% of crystal violet solution (100 μl) and re-incubated at room temperature for 30 min. Furthermore, the additional crystal violet solution from the plate was cast off and the disc was washed with distilled water, followed by air drying. Then, 100 μl of 95% ethanol was added into the well to solubilize stained crystal violet, and the absorbance was measured using a TRIAD Multimode Reader at 540 nm against a blank.[56]

4.4 | DNA gyrase inhibitory activity

The synthesized compounds were screened for their potency against DNA gyrase-A of *S. aureus* according to the previously reported method.[57] Briefly, the colony of *S. aureus* was cultured in a medium (consisting of 2 g yeast extract, 10 g polypeptone, 1.2 g $(NH_4)_2SO_4$, 8 g Na_2HPO, 2 g KH_2PO_4, 0.2 g $MgSO_4$, 4 g glucose in 1 L distilled water). The purification, supercoiling, and decatenation of *S. aureus* were executed according to the reported method of Blanche et al.,[58] and the IC_{50} (in μg/ml) was determined through a dose–response curve.

4.5 | 3D QSAR analysis

3D QSAR studies were performed using the "Cinderella Shoe" (CiS) method[59] and continual molecular interior (CoMIn) algorithms.[60,61] Cinderella Shoe[59] is a complementary pseudoatomic receptor model used for calculating contributions of ligands' topographies and defining potentials at the points of molecular space obtained in the generalized superimposed lattice of the entire data set. In this way, a reliable pattern for pharmacophore, antipharmacophore, and ballast fragments of ligands can be obtained very fast. The CiS method uses 10 splits for validation, where each contains 80% training and 20% for testing data set. Each split is randomly selected and follows the decoy set in both training and testing data sets in this variant.[60,62–64]

Recently introduced RDF descriptor weighted by the number of valence shell electrons ($g(r)$) was used to design QSAR model correlating it with the ligands' potential to inhibit DNA gyrase (IC_{50} values).[65,66] For each optimized structure, hydrogen atoms were removed, and $g(r)$ was calculated. It is represented as a vector of a predetermined size

$$g(r) = \sum_{i=1}^{N-1} \sum_{j>i}^{N} p_i p_j e^{-a_{ij}^{-2/3}(r_{ij}-r)^2} \quad (2)$$

with elements calculated at a discrete distance r and a distance step of 0.1 Å. a_{ij} is the sum of atomic polarizabilities of atoms i and j, r_{ij} the distance between atoms i and j, N is the number of atoms in a molecule, and the pre-exponential factors p_i and p_j account for the number of outer electrons of the ith and jth atoms, correspondingly. Atomic polarizabilities are calculated within the MERA model.[67–69] Multiple linear regression algorithm with the forward stepwise method was exploited to build a QSAR model correlating the RDF-based descriptors and IC_{50} values.

4.6 | Absorption, distribution, metabolic liability prediction, and excretion studies

The ADME computations for log P, TPSA, Lipinski violation, H donor, H acceptor, water solubility score, gastrointestinal absorption score, and the possibility of metabolism at different sites of CYP450 were carried out using online platform www.chemosophia.com,[70] pkCSM predictor,[44] and Swissadme.ch.[71] Furthermore, participation of different atoms of the derivatives in metabolic liability at cytochrome P450 was determined using the web server of RS-Predictor.[45]

4.7 | Molecular docking

AutoDockTools 4 script prepare_ligand4.py[72] was used to prepare the optimized molecules for docking, saving them in the pdbqt file format. The crystal structure of the DNA gyrase complexed with drug ciprofloxacin and DNA (PDB ID: 2XCT) was downloaded from Protein Data Bank.[73] Chimera 1.14[74] was used for visual inspection of the structure. MODELLER web interface[75] was used to model missing residues. AutoDockTools graphical interface was used to add Gasteiger charges to each atom, to merge nonpolar hydrogens, for determination of atom types, and to save prepared receptor structure in pdbqt file format. The center of the grid box was set at the center of the mass of the ciprofloxacin (belonging to the B chain), with Cartesian coordinates 2.84, 43.71, and 68.66 Å, whereas the size of the grid box was $24 \times 20 \times 30$ Å^3. The exhaustiveness was set to 100. Docking was performed using the AutoDock Vina software[76] on an Intel i7-6700 machine with 16 GB of RAM.

4.8 | Fingerprinting

Extended connectivity 2D molecular fingerprints (ECFP) were calculated for all molecules using RDKit (2020.03.1).[77] The molecular similarity was estimated on the basis of the Tanimoto coefficient[78]

$$T_c(A, B) = \frac{c}{a + b - c} \quad (3)$$

where a and b are numbers of features present in compounds A and B, respectively, whereas c is the number of features shared by compounds A and B. The Tanimoto coefficient varies in range from 0 to 1, with 0 representing minimum and 1 representing maximum similarity between compounds A and B.

The ECFP for synthesized molecules was compared with calculated ECFP for 430 compounds from the ChEMBL database tested against *S. aureus* DNA gyrase activity (release version 5.1.5).[79,80]

ACKNOWLEDGMENTS

The authors are also sincerely thankful to the Department of Pharmaceutical Sciences, SHUATS, Uttar Pradesh, India, and Laboratory of Computational Modelling of Drugs, Higher Medical and Biological School, South Ural State University, Chelyabinsk, Russia, for experimental and computational research facilities. A part of the work was supported by Act 211 Government of the Russian Federation, contract 02.A03.21.0011, and by the Ministry of Science and Higher Education of Russia (Grant FENU-2020-0019).

CONFLICTS OF INTERESTS

The authors declare that there are no conflicts of interests.

ORCID

Prateek Pathak https://orcid.org/0000-0002-6160-9755
Jurica Novak https://orcid.org/0000-0001-5744-6677
Parjanya K. Shukla https://orcid.org/0000-0003-1202-0343
Maria Grishina http://orcid.org/0000-0002-2573-4831
Vladimir Potemkin http://orcid.org/0000-0002-5244-8718
Amita Verma http://orcid.org/0000-0001-6653-7335

REFERENCES

[1] T. A. Keating, J. V. Newman, N. B. Olivier, L. G. Otterson, B. Andrews, P. A. Boriack-Sjodin, J. N. Breen, P. Doig, J. Dumas, E. Gangl, O. M. Green, S. Y. Guler, M. F. Hentemann, D. Joseph-Mccarthy, S. Kawatkar, A. Kutschke, J. T. Loch, A. R. McKenzie, S. Pradeepan, S. Prasad, G. Martínez-Botella, *ACS Chem. Biol.* **2012**, *7*, 1866.
[2] B. Aslam, W. Wang, M. I. Arshad, M. Khurshid, S. Muzammil, M. H. Rasool, M. A. Nisar, R. F. Alvi, M. A. Aslam, M. U. Qamar, M. K. F. Salamat, Z. Baloch, *Infect. Drug Resist.* **2018**, *11*, 1645.
[3] N. R. Naylor, R. Atun, N. Zhu, K. Kulasabanathan, S. Silva, A. Chatterjee, G. M. Knight, J. V. Robotham, *Antimicrob. Resist. Infect. Control* **2018**, *7*, 58.
[4] S. P. Kawatkar, T. A. Keating, N. B. Olivier, J. N. Breen, O. M. Green, S. Y. Guler, M. F. Hentemann, J. T. Loch, A. R. McKenzie, J. V. Newman, L. G. Otterson, G. Martínez-Botella, *J. Med. Chem.* **2014**, *57*, 4584.
[5] F. Gao, T. Wang, J. Xiao, G. Huang, *Eur. J. Med. Chem.* **2019**, *173*, 274.
[6] M. Hussain, T. Qadri, Z. Hussain, A. Saeed, P. A. Channar, S. A. Shehzadi, M. Hassan, F. A. Larik, T. Mahmood, A. Malik, *Heliyon* **2019**, *5*, 1.
[7] Centers for Disease Control and Prevention, *Antibiotic Resistance Threats in the United States*, 2019, U.S. Department of Health and Human Services, CDC, Atlanta, GA **2019**.
[8] M. Wahab Khan, M. Jahangir Alam, M. A. Rashid, R. Chowdhury, *Bioorg. Med. Chem.* **2005**, *13*, 4796.
[9] F. Collin, S. Karkare, A. Maxwell, *Appl. Microbiol. Biotechnol.* **2011**, *92*, 479.
[10] A. J. Schoeffler, J. M. Berger, *Q. Rev. Biophys.* **2008**, *41*, 41.
[11] A. Merino, K. R. Madden, W. S. Lane, J. J. Champoux, D. Reinberg, *Nature* **1993**, *365*, 227.
[12] T. Khan, K. Sankhe, V. Suvarna, A. Sherje, K. Patel, B. Dravyakar, *Biomed. Pharmacother.* **2018**, *103*, 923.
[13] T. Kirchhausen, J. C. Wang, S. C. Harrison, *Cell* **1985**, *41*, 933.
[14] A. Maxwell, D. Lawson, *Curr. Top. Med. Chem.* **2005**, *3*, 283.
[15] D. B. Tiz, Ž. Skok, M. Durcik, T. Tomašič, L. P. Mašič, J. Ilaš, A. Zega, G. Draskovits, T. Révész, Á. Nyerges, C. Pál, C. D. Cruz, P. Tammela, D. Žigon, D. Kikelj, N. Zidar, *J. Med. Chem.* **2019**, *167*, 269.
[16] J. C. Wang, *Untangling the Double Helix: DNA Entanglement and the Action of the DNA Topoisomerases*, Cold Spring Harbor Laboratory Press, Cold Spring Harbor, NY **2009**.
[17] C. Gao, L. Chang, Z. Xu, X.-F. Yan, C. Ding, F. Zhao, X. Wu, L.-S. Feng, *Eur. J. Med. Chem.* **2019**, *163*, 404.
[18] B. Meunier, *Acc. Chem. Res.* **2008**, *41*, 69.
[19] S. M. Shaveta, P. Singh, *Eur. J. Med. Chem.* **2016**, *124*, 500.
[20] R. Domalaon, T. Idowu, G. G. Zhanel, F. Schweizer, *Clin. Microbiol. Rev.* **2018**, *31*, 1.
[21] B. Kaproń, J. J. Łuszczki, A. Płazińska, A. Siwek, T. Karcz, A. Gryboś, G. Nowak, A. Makuch-Kocka, K. Walczak, E. Langner, K. Szalast, S. Marciniak, M. Paczkowska, J. Cielecka-Piontek, L. M. Ciesla, T. Plech, *Eur. J. Pharm. Sci.* **2019**, *129*, 42.
[22] S. A. Shahzad, M. Yar, Z. A. Khan, L. Shahzadi, S. A. R. Naqvi, A. Mahmood, S. Ullah, A. J. Shaikh, T. A. Sherazi, A. T. Bale, J. Kukułowicz, M. Bajda, *Bioorg. Chem.* **2019**, *85*, 209.
[23] H. A. M. El-Sherief, B. G. M. Youssif, S. N. Abbas Bukhari, A. H. Abdelazeem, M. Abdel-Aziz, H. M. Abdel-Rahman, *Eur. J. Med. Chem.* **2018**, *156*, 774.
[24] K. Wittine, M. Stipković Babić, D. Makuc, J. Plavec, S. Kraljević Pavelić, M. Sedić, K. Pavelić, P. Leyssen, J. Neyts, J. Balzarini, M. Mintas, *Bioorg. Med. Chem.* **2012**, *20*, 3675.
[25] S. Zhang, Z. Xu, C. Gao, Q.-C. Ren, L. Chang, Z.-S. Lv, L.-S. Feng, *Eur. J. Med. Chem.* **2017**, *138*, 501.

[26] P. Pathak, P. K. Shukla, V. Naumovich, M. Grishina, A. Verma, V. Potemkin, *Arch. Pharm. (Weinheim)* **2020**, *353*, 1.
[27] R. Y. Jin, C. Y. Zeng, X. H. Liang, X. H. Sun, Y. F. Liu, Y. Y. Wang, S. Zhou, *Bioorg. Chem.* **2018**, *80*, 253.
[28] J. Xu, Y. Cao, J. Zhang, S. Yu, Y. Zou, X. Chai, Q. Wu, D. Zhang, Y. Jiang, Q. Sun, *Eur. J. Med. Chem.* **2011**, *46*, 3142.
[29] S. Eswaran, A. V. Adhikari, N. S. Shetty, *Eur. J. Med. Chem.* **2009**, *44*, 4637.
[30] R. Kharb, P. C. Sharma, M. S. Yar, *J. Enzyme Inhib. Med. Chem.* **2011**, *26*, 1.
[31] D. R. Godhani, A. A. Jogel, P. B. Dobariya, A. M. Sanghani, *J. Saudi Chem. Soc.* **2016**, *20*, S523.
[32] V. P. M. Rahman, S. Mukhtar, W. H. Ansari, G. Lemiere, *Eur. J. Med. Chem.* **2005**, *40*, 173.
[33] P. Pathak, P. K. Shukla, V. Naumovich, M. Grishina, V. Potemkin, A. Verma, *Synth. Commun.* **2019**, *49*, 2725.
[34] S. Raza, S. P. Srivastava, D. S. Srivastava, A. K. Srivastava, W. Haq, S. B. Katti, *Eur. J. Med. Chem.* **2013**, *63*, 611.
[35] R. K. Rawal, Y. S. Prabhakar, S. B. Katti, E. De Clercq, *Bioorg. Med. Chem.* **2005**, *13*, 6771.
[36] C. J. Andres, J. J. Bronson, S. V. D′Andrea, M. S. Deshpande, P. J. Falk, K. A. Grant-Young, W. E. Harte, H.-T. Ho, P. F. Misco, J. G. Robertson, D. Stock, Y. Sun, A. W. Walsh, *Bioorg. Med. Chem. Lett.* **2000**, *10*, 715.
[37] K. Babaoglu, M. A. Page, V. C. Jones, M. R. McNeil, C. Dong, J. H. Naismith, R. E. Lee, *Bioorg. Med. Chem. Lett.* **2003**, *13*, 3227.
[38] A. Masih, J. K. Shrivastava, H. R. Bhat, U. P. Singh, *Chem. Biol. Drug Des.* **2020**, *96*, 861.
[39] M. A. Salem, A. Ragab, A. A. Askar, A. El-Khalafawy, A. H. Makhlouf, *Eur. J. Med. Chem.* **2020**, *188*, 1.
[40] C. A. Lipinski, *Drug Discov. Today Technol.* **2004**, *1*, 337.
[41] N. Das, J. Madhavan, A. Selvi, D. Das, *3 Biotech.* **2019**, *9*, 231.
[42] C. H. Ballow, G. W. Amsden, *Ann. Pharmacother.* **1992**, *26*, 1253.
[43] C. Csongradi, J. du Plessis, M. E. Aucamp, M. Gerber, *J. Pharm. Biopharm.* **2017**, *114*, 96.
[44] D. E. V. Pires, T. L. Blundell, D. B. Ascher, *J. Med. Chem.* **2015**, *58*, 4066.
[45] J. Zaretzki, C. Bergeron, P. Rydberg, T. Huang, K. P. Bennett, C. M. Breneman, *J. Chem. Inf. Model.* **2011**, *51*, 1667.
[46] New Zealand Medicines and Medical Devices Safety Authority, *Prescriber Update* **2014**, *35*, 4.
[47] Y. C. Chen, *Trends Pharmacol. Sci.* **2015**, *36*, 78.
[48] S. Riniker, G. A. Landrum, *J. Cheminf.* **2013**, *5*, 26.
[49] X. H. Liu, P. Cui, B. A. Song, P. S. Bhadury, H. L. Zhu, S. F. Wang, *Bioorg. Med. Chem.* **2008**, *16*, 4075.
[50] J. B. Patel, F. R. Cockerill III, P. A. Bradford, G. M. Eliopoulos, J. A. Hindler, S. G. Jenkins, J. S. Lewis II, B. Limbago, L. A. Miller, D. P. Nicolau, M. Powell, J. M. Swenson, M. M. Traczewski, J. D. Turnidge, M. P. Weinstein, B. L. Zimmer, *Clinical Laboratory Standards Institute.* **2015**, *32*(2), 187. https://clsi.org/media/1632/m07a10_sample.pdf
[51] P. Pathak, A. Thakur, H. R. Bhat, U. P. Singh, *J. Heterocycl. Chem.* **2015**, *52*, 1108.
[52] P. Prateek, A. Thakur, P. K. Shukla, *Int. J. ChemTech Res.* **2016**, *9*, 261.
[53] M. Sandasi, C. M. Leonard, A. M. Viljoen, *Food Control* **2008**, *19*, 1070.
[54] A. Kamal, S. M. A. Hussaini, M. L. Sucharitha, Y. Poornachandra, F. Sultana, C. G. Kumar, *Org. Biomol. Chem.* **2015**, *13*, 9388.
[55] A. Kamal, A. Rahim, S. Riyaz, Y. Poornachandra, M. Balakrishna, C. G. Kumar, S. M. A. Hussaini, B. Sridhar, P. K. Machiraju, *Org. Biomol. Chem.* **2015**, *13*, 1347.
[56] D. Djordjevic, M. Wiedmann, L. A. McLandsborough, *Appl. Environ. Microbiol.* **2002**, *68*, 2950.
[57] M. S. Osburne, W. M. Maiese, M. Greenstein, *J. Antibiot. (Tokyo)* **1993**, *46*, 1764.
[58] F. Blanche, B. Cameron, F. X. Bernard, L. Maton, B. Manse, L. Ferrero, N. Ratet, C. Lecoq, A. Goniot, D. Bisch, J. Crouzet, *Antimicrob. Agents Chemother.* **1996**, *40*, 2714.
[59] V. Potemkin, O. Galimova, M. Grishina, *Drugs Future* **2010**, *35*, 14.
[60] A. V. Potemkin, M. A. Grishina, V. A. Potemkin, *Curr. Drug. Discov. Technol.* **2017**, *14*, 181.
[61] V. Potemkin, M. Grishina, *Curr. Med. Chem.* **2018**, *25*, 3526.
[62] V. A. Potemkin, M. A. Grishina, *J. Comput.-Aided. Mol. Des.* **2008**, *22*, 489.
[63] V. Potemkin, M. Grishina, *Drug Discov. Today* **2008**, *13*, 952.
[64] P. Pathak, V. Naumovich, M. Grishina, P. K. Shukla, A. Verma, V. Potemkin, *Arch. Pharm. (Weinheim)* **2019**, *352*, 1.
[65] J. Novak, M. A. Grishina, V. A. Potemkin, J. Gasteiger, *Future Med. Chem.* **2020**, *12*, 299.
[66] J. Novak, M. A. Grishina, V. A. Potemkin, *Future Med. Chem.* **2020**, *12*, 1025.
[67] V. Potemkin, E. Bartashevich, A. Belik, *J. Phys. Chem. A* **1996**, *70*, 411.
[68] V. A. Potemkin, A. A. Pogrebnoy, M. A. Grishina, *J. Chem. Inf. Model.* **2009**, *49*, 1389.
[69] V. Potemkin, A. Potemkin, M. Grishina, *Curr. Top. Med. Chem.* **2019**, *18*, 1955.
[70] V. Potemkin, M. Grishina, **2018**. www.cheosophia.com (accessed: October 2020).
[71] A. Daina, O. Michielin, V. Zoete, *Sci. Rep.* **2017**, *7*, 1.
[72] G. M. Morris, R. Huey, W. Lindstrom, M. F. Sanner, R. K. Belew, D. S. Goodsell, A. J. Olson, *J. Comput. Chem.* **2009**, *30*, 2785.
[73] B. D. Bax, P. F. Chan, D. S. Eggleston, A. Fosberry, D. R. Gentry, F. Gorrec, I. Giordano, M. M. Hann, A. Hennessy, M. Hibbs, J. Huang, E. Jones, J. Jones, K. K. Brown, C. J. Lewis, E. W. May, M. R. Saunders, O. Singh, C. E. Spitzfaden, C. Shen, A. Shillings, A. J. Theobald, A. Wohlkonig, N. D. Pearson, M. N. Gwynn, *Nature* **2010**, *466*, 935.
[74] E. F. Pettersen, T. D. Goddard, C. C. Huang, G. S. Couch, D. M. Greenblatt, E. C. Meng, T. E. Ferrin, *J. Comput. Chem.* **2004**, *25*, 1605.
[75] B. Webb, A. Sali, *Curr. Protoc. Bioinf.* **2016**, *54*, 54. https://doi.org/10.1002/cpbi.3
[76] O. Trott, A. J. Olson, *J. Comput. Chem.* **2009**, *31*, 455.
[77] G. Landrum, RDKit: Open-source cheminformatics. **2006**. https://www.rdkit.org/ (accessed: November 2020).
[78] D. Bajusz, A. Rácz, K. Héberger, *J. Cheminf.* **2015**, *7*, 20.
[79] D. S. Wishart, Y. D. Feunang, A. C. Guo, E. J. Lo, A. Marcu, J. R. Grant, T. Sajed, D. Johnson, C. Li, Z. Sayeeda, N. Assempour, I. Iynkkaran, Y. Liu, A. Maciejewski, N. Gale, A. Wilson, L. Chin, R. Cummings, D. Le, A. Pon, C. Knox, M. Wilson, *Nucleic Acids Res.* **2018**, *46*, D1074.
[80] M. Davies, M. Nowotka, G. Papadatos, N. Dedman, A. Gaulton, F. Atkinson, L. Bellis, J. P. Overington, *Nucleic Acids Res.* **2015**, *43*, W612.

How to cite this article: P. Pathak, J. Novak, P. K. Shukla, M. Grishina, V. Potemkin, A. Verma, *Arch. Pharm.* **2021**, e2000473.